Groundwater Modelling For Recharge Estimation Using Satellite Based Evapotranspiration

Salland Case, The Netherlands

MAHMOUD SOHEILI

March, 2014

SUPERVISORS:
Dr. ing. T.H.M. (Tom) Rientjes
Dr. ir. C. (Christiaan) van der Tol

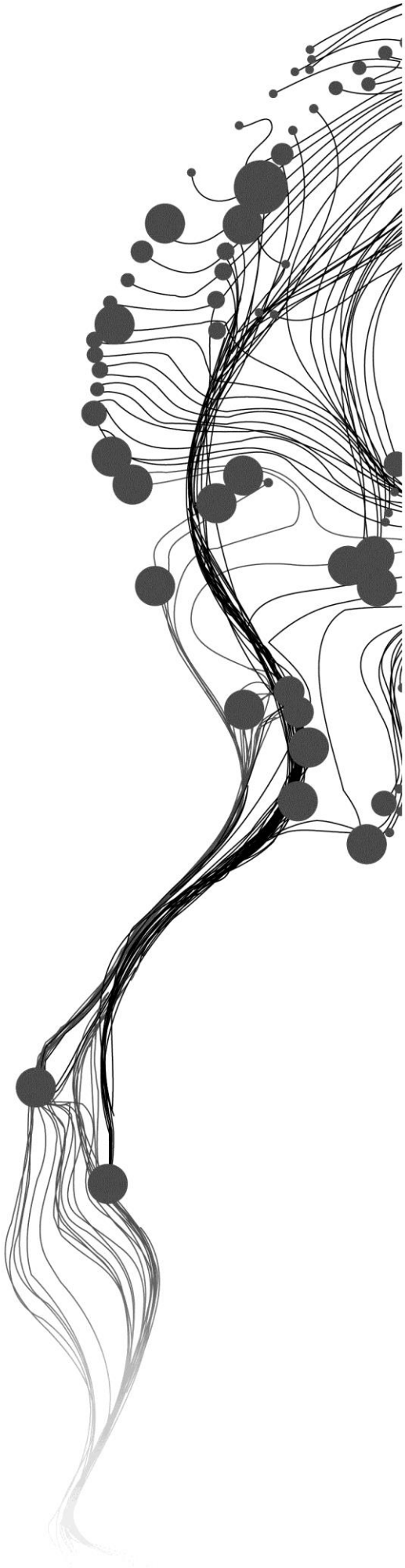

Groundwater Modelling For Recharge Estimation Using Satellite Based Evapotranspiration

Salland Case, The Netherlands

MAHMOUD SOHEILI

Enschede, The Netherlands, March, 2014

Thesis submitted to the Faculty of Geo-Information Science and Earth Observation of the University of Twente in partial fulfilment of the requirements for the degree of Master of Science in Geo-information Science and Earth Observation.

Specialization:
Water Resources and Environmental Management (WREM)

SUPERVISORS:
Dr. ing. T.H.M. (Tom) Rientjes
Dr. ir. C. (Christiaan) van der Tol

THESIS ASSESSMENT BOARD:
Prof. Dr. Ing. W. Verhoef (Chair)
Ir. M. Ter Haar (External Examiner, Waterschap Groot Salland)

DISCLAIMER

This document describes work undertaken as part of a programme of study at the Faculty of Geo-Information Science and Earth Observation of the University of Twente. All views and opinions expressed therein remain the sole responsibility of the author, and do not necessarily represent those of the Faculty.

…and of water We have made every living thing…

The Noble Quran [21:30]

To my beloved parents...

ABSTRACT

Groundwater movement is influenced by several factors and processes in the hydrological cycle, from which, recharge is of high relevance. Since the amount of aquifer extractable water directly relates to the recharge amount, estimation of recharge is a perquisite of groundwater resources management. Recharge is highly affected by water loss mechanisms the major of which is actual evapotranspiration (ETa). It is, therefore, essential to have detailed assessment of ETa impact on groundwater recharge.

The objective of this study was to evaluate how recharge was affected when satellite-based evapotranspiration was used instead of in-situ based ETa in the Salland area, the Netherlands.

The Methodology for Interactive Planning for Water Management (MIPWA) model setup which includes a groundwater model for the northern part of the Netherlands was used for recharge estimation. Precipitation and Makkink-based potential evaporation data collected from 01 May 2012 to 30 April 2013 for the Salland region daily were used. The Surface Energy Balance Algorithm for Land (SEBAL) based actual evapotranspiration maps from Waterschap Groot Salland were also used.

Comparison of SEBAL based ETa estimates with in-situ abased estimates in the Netherlands showed that these SEBAL estimates were not reliable. As such results could not serve for calibrating root zone parameters in the CAPSIM model. The annual cumulative ETa map produced by the model showed that the maximum amount of evapotranspiration occurs in mixed forest areas in the northeast and a portion of central parts. Estimates ranged from 579 mm to a minimum of 0 mm in the highest elevated areas with woody vegetation in the southeast of the region.

Variations in mean seasonal hydraulic head and groundwater level for each layer showed that the hydraulic gradient follows elevation in the Salland area from southeast (maximum) to northwest (minimum) of the region which depicts the groundwater flow direction.

The mean seasonal water balance in CAPSIM part was evaluated to represent recharge estimation in the first layer. The highest recharge estimated flux was for autumn season and was equal to 28 m^3/day whereas the lowest flux was -5.6 m^3/day in spring. The spatial distribution also shows that maximum groundwater recharge estimated was in the southeast of the region due to the lack of vegetation cover and deep groundwater levels. Lowest groundwater recharge estimated in urban and agricultural areas in the northwest of the Salland area.

The overall conclusion of this study is that groundwater level fluctuations in the Salland area are affected by seasonal climatic variations specially precipitation and evapotranspiration. Such however was not supported by the SEBAL images which proved to be unreliable.

Key words: Groundwater recharge, Actual evapotranspiration, MIPWA, SEBAL, Salland

ACKNOWLEDGEMENTS

Laudation to the God of majesty and glory! Obedience to him is a cause of approach and gratitude in increase of benefits. - Saadi Shirazi-

First and foremost, I am grateful to my God, the One Who opened the door of goodness and blessings to me while all the other doors were locked. The One Who had never left me alone and His grace and kindness is an approval to this verse of Noble Quran: "the Hand of Allah is above their hands" [48:10].

I am thankful to my -dearer to me than my own soul- parents and believe that whatever I achieved is the fruit of their efforts and their everlasting kind supports. I appreciate my brothers; Ahmad and his family and Mohammad; also all of my uncles; Ali (the one who encouraged me a lot before he passed away), Mohammad, Hossein, Hassan; and my aunts; Azam, Ezzat, Mahin, Shahin, Razieh, Marzieh and their families whom, being here far from them, I understood their true value and all of my relatives who remembered me in these 18 months.

I would like to express my gratefulness to Tom Rientjes -my first supervisor- from whom, I have learned a lot, not only in the thesis period but all the way back throughout the courses, when his invaluable guidance kept me on track to the success destination. I am thankful to Christiaan van der Tol who had a great impact on my thesis work, to Arno van Lieshout, who has always helped me in these 18 months and to Marloes ter Haar and her colleagues who kindly helped in solving modelling problems.

Among my friends in Iran, I am grateful to the following: Hadi Nikoo who have been my truly honest friend both in hardship and good times; Hossein Yaghoubi, who have been my constant encourager; Mohammad Afzali who have always been on my side to further my education, Sayed Mahdi Mousavinia, to whom, I am truly indebted for his kindness in the long years of our friendship; Ehsan Ebrahimi who I received his guidance and his helping conversations here far from home and to Azizallah Izady for all of his helps during Bachelors and Masters period.

I appreciate the kindness of my dear friends here: lovely Mahdi Beheshti, who had been by my side from the very first moments I entered Enschede to this day and had always been my buddy and friend in the most difficult moments; Majid, Hamed, Alireza, Meisam and Jamal who have been my point of trust and played the role as experienced older brothers; dear Sayed Salman, my fellow townsman and friend from Mashhad, who accompanied me like a brother both while he was here and when he returned back to Iran and his constant helps in my work cannot ever be compensated; the wives of these friends, whom their reception and hospitality, made my days apart from family more bearable; and Mehdi Aminipouri and his lovely family, who although left us too soon, his words and helps were and will always stay with me.

I am also grateful to Hamed, Milad, Vahid, Saeid, Hossein(s) and all my Iranian new-comer friends in ITC, who have made a wonderful Iranian society here in the Netherlands; and to Bagher, his wife and Fatemeh Mahmoudi for being great neighbors. I especially appreciate Bagher's educational guidance and his helps in doing the work quickly.

I am thankful to my wonderful classmates, Boss "Amr" for all of his helps in the MSc courses; Achmad Ervan for his brotherly conversations; my three Ethiopian friends: Asmelash, Mastawesha and Teshale with whom I had enjoyable time; Jonathan Edika, Chenyang and all ITC friends who made good memories; and "Omar" who his brotherly helps and guidance were great support in finishing the job on time.

And finally I am grateful to Erasmus Mundus Foundation, Ferdowsi University of Mashhad and ITC who provided me with great learning environments; and to friendly people of the Netherlands, whom with their enjoyable hospitality, provided me with a nice and cheerful place for living and learning and left me with enjoyable life souvenirs.

TABLE OF CONTENTS

List of figures vii
List of tables ix
List of abbreviations x
List of symbols xi
1. Introduction 13
1.1. Background 13
1.2. Problem statement 14
1.3. Research Objective 15
1.4. Research Questions 15
2. Literature review and MIPWA description 17
2.1. Recharge estimation and remote sensing 17
2.2. Groundwater modelling 20
2.3. MIPWA model 20
2.4. CAPSIM part of MIPWA model 24
3. Study area 27
3.1. Study Area 27
3.2. Area description 28
3.3. Distribution of Soil type 29
3.4. Geo-hydrological parameters and system representation 30
4. data collection 33
4.1. CAPSIM 33
4.2. Precipitation 34
4.3. Evaporation 35
.4.4 Actual Evapotranspiration 37
5. Methodology 39
5.1. Groundwater flow equation 40
5.2. MODFLOW 41
6. Results and discussion 45
6.1. Analysis of SEBAL based ETa maps 45
6.2. Analysis of MIPWA-CAPSIM based ETa map 50
6.3. Feddes equation parameters in the Model 51
6.4. Analysis of Classified MIPWA-CAPSIM based cumulative ETa map 51
6.5. Hydraulic head and groundwater level 54
6.6. CAPSIM waterbalance and recharge estimation 56
7. Conclusions and Recommendations 59
7.1. Conclusions 59
7.2. Recommendations 60

List of references 61
Appendices 64

LIST OF FIGURES

Figure 2-1, MIPWA project area (dark grey) and the total modelled area (shaded) (Berendrecht et al, 2007) 21
Figure 2-2, Processes described by the MODFLOW-SIMGRO model (Berendrecht et al, 2007) 22
Figure 2-3, Concept of iMOD processing 23
Figure 2-4, CAPSIM component of MIPWA model 24
Figure 3-1, Location of Groot Salland in the Netherlands (Black boundary) 27
Figure 3-2, Management of study area (www.wgs.nl) 28
Figure 3-3, Digital elevation map of the study area 28
Figure 3-4, Distribution of Soil type map of Salland area 29
Figure 3-5, Cross-section of 7 separating geologic layers. 30
Figure 3-6, Model layers in the MIPWA approach for the Salland study area 31
Figure 4-1, Thiessen polygon of KNMI meteorological stations 34
Figure 4-2, Precipitation of Zwolle station 34
Figure 4-3, Location of Marknesse station 35
Figure 4-4, Location of Heino station 35
Figure 4-5, The reducing function of water absorption by plants in different matrix suction conditions .. 37
Figure 4-6, Daily SEBAL-based ETa map for 14st of May 2012 38
Figure 4-7, Daily SEBAL-based ETa map for 28st of May 2012 38
Figure 5-1, Methodology flow chart 39
Figure 5-2 Grid structure of the model domain area 42
Figure 6-1, Mean SEBAL-based ETa for spring 45
Figure 6-2, Mean SEBAL-based ETa for summer 45
Figure 6-3, Mean SEBAL-based ETa for autumn 46
Figure 6-4 , Difference map of ETa between summer and spring seasons 46
Figure 6-5 , Difference map of ETa between summer and autumn seasons 46
Figure 6-6, Relation between Penman evaporation and actual evapotranspiration (de Vries 1974) for (1950-1970). 47
Figure 6-7, Relation between Penman evaporation and actual evapotranspiration (de Vries 1974) for (1950-1970). 48
Figure 6-8, comparing KNMI ETa and SEBAL-based ETa 49
Figure 6-9, Cumulative ETa map for 2012-2013 provided by MIPWA-CAPSIM 50
Figure 6-10, SEBAL-based cumulative ETa map for 8 months 50
Figure 6-11, Classified cumulative ETa map provided by MIPWA for one year 51
Figure 6-12, Satellite images of land use in Salland area 53
Figure 6-13, Mean hydraulic head of layer 1 for spring 54
Figure 6-14, Mean hydraulic head of layer 1 for summer 54
Figure 6-15, Mean hydraulic head of layer 1 for autumn 54
Figure 6-16, Mean hydraulic head of layer 1 for winter 54
Figure 6-17, Mean groundwater level of layer 1 for spring 55
Figure 6-18, Mean groundwater level of layer 1 for summer 55
Figure 6-19, Mean groundwater level of layer 1 for autumn 55
Figure 6-20, Mean groundwater level of layer 1 for winter 55
Figure 6-21, Mean water balance in CAPSIM for spring 56
Figure 6-22, Mean water balance in CAPSIM for summer 56

Figure 6-23, Mean water balance in CAPSIM for autumn 57
Figure 6-24, Mean water balance in CAPSIM for winter 57
Figure 6-25, Hydraulic head for steady-state model 58
Figure 6-26, Recharge estimated value for steady-state model 58

LIST OF TABLES

Table 4-1, Names and numbers of the KNMI precipitation stations 34
Table 4-2, Crop factors 35
Table 4-3, KNMI stations information 35
Table 6-1, Mean actual evapotranspiration for each season 46
Table 6-2, Mean monthly Makkink evaporation (Hiemstra and Sluiter, 2011) and its ETa (de Vries, 1979) 48
Table 6-3, The SEABAL-based average ET_a values for 8 months 49
Table 6-4, Statistic of cumulative ETa maps provided by MIPWA-CAPSIM and SEBAL-based 50
Table 6-5, Statistics of mean seasonal hydraulic head maps 55
Table 6-6, Statistics of mean seasonal groundwater level maps 56
Table 6-7, Statistics of mean seasonal water balance in CAPSIM part 57
Table 6-8, Statistics of hydraulic head map (steady-state) 58
Table 6-9, Statistics of recharge map (steady-state) 58

LIST OF ABBREVIATIONS

RS	Remote Sensing
GIS	Geographic Information Systems
SEBAL	Surface Energy Balance Algorithm for Land
MIPWA	Methodology for Interactive Planning for Water Management
iMOD	Interactive Modelling
GMS	Groundwater Modelling System
KNMI	Royal Netherlands Meteorological Institute
USGS	United States Geological Survey
IO	Input-Output
PRF	iMOD Preference File
IMF	iMOD Meta File
IDF	iMOD Data File
IPF	iMOD Point File
IFF	iMOD Flow File
ISG	iMOD Segment File
GEN	ESRI Generate File
DAT	ESRI Generate File
ASC	ERSI Raster File
LEG	iMOD Legend File
CLR	iMOD Colour File
DLF	File containing color information to display boreholes
CRD	iMOD Coordinate File
UTC	Coordinated Universal Time
FD	Finite differences
SEBAL	Surface Energy Balance Algorithm for Land
DEM	Digital Elevation Model
IO	Input-output

LIST OF SYMBOLES

Symbols	Description	Unit
ET	Evapotranspiration	[mm day-1]
ETa	Actual Evapotranspiration	[mm day-1]
ETp	Potential Evapotranspiration	[mm day-1]
Ta	Actual Transpiration	[mm day-1]
Tp	Potential Transpiration	[mm day-1]
Z_r	Height of roots	[mm]
h	Pressure Head	[mm]
$\alpha(h)$	Reduction coefficient for root water uptake	
S	Root Water Uptake	[day-1]
S_{max}	Maximum Root Water Uptake	[day-1]

1. INTRODUCTION

1.1. Background

Renewable water resources require high efficiency in water consumption to guarantee its sustainable use. Managing renewable water resources involves careful planning by water managers and decision-makers but also careful consideration by researchers and experts. Often groundwater resources are used to meet water demands by urban, industrial and agricultural uses. For optimal management of groundwater resources, accurate information on water inputs and outputs in the groundwater basin is important so that the long-term behaviour of the aquifer and its sustainable yield can be estimated and monitored. Investigations on groundwater recharge and related system characteristics commonly are performed by hydro-geologists, hydrologists and climatologist (Kumar 1977).

Groundwater movement occurs under the control of several factors and processes including recharge which is one of the most important processes in the hydrological cycle. Recharge itself is influenced by a large number of factors that relate to meteorology, soils, surface cover, elevation and geology. This causes that recharge and groundwater levels differ both in time and space (Bouwer 1978; Shukla & Jaber 2006; Sumioka & Bauer 2003). From the water supply side for a groundwater system, availability of groundwater resources mainly depends on the groundwater recharge. Efficient and sustainable groundwater resources management is largely dependent on the quantification of groundwater recharge which is defined as any form of water movement from the land surface to the groundwater. Groundwater recharge may occur both naturally through the water cycle or artificially by human-induced processes. By the many factors involved, groundwater recharge estimation is difficult. However, obtaining reliable quantitative estimates are essential in maximizing the potential of available, but often limited, groundwater resources. This requires a clear conceptual understanding of key processes of specific magnitude and time-space variability. For quantitative assessments such as modelling, relevant data should be collected and assimilated.

Recharge is largely affected by precipitation (i.e., rainfall and snowfall) that has a central role in quantitative assessments in hydrological and hydrogeological studies (Xi et al. 2008). Rainfall and snowmelt are the two major forms of water input to the hydrologic system. The main water outflow of the system is runoff that causes stream flow, and evaporation as well as plants transpiration. Over the surface, precipitation may generate overland flow that is added to the streams. In natural catchment systems, most precipitation water infiltrates the subsurface and eventually may recharge the saturated subsurface (i.e., groundwater system). Subsurface flows as generated by infiltration water, may contribute to channel flows by interflow, lateral flow and base flow. Recharge is also affected by actual evaporation and transpiration (ET) which is the amount of water evaporated from the soil surface and transpired from vegetation. It is a major process in hydrological cycle and is one of the key processes in water resources management (Gao et al., 2008). ET has a significant effect on hydrological conditions and makes its computation necessary in groundwater assessments and modelling. Calculation of ET often is complicated due to the complexity of the parameter itself and, often, the lack of required information for accurate spatio-temporal modelling (Brutsaert, 1982).

Alternative to the use of in-situ data is the use of satellite imagery which may provide a significant amount of data at low cost and high compatibility with areas being studied. The analysis of these images for vegetation land cover and ET estimates in different time intervals and places, provide valuable information in water resources modelling. Therefore, nowadays, many efforts report on use and integration of satellite imagery in hydrological modelling.

Several attempts have been made to methodological approaches to validate ET estimations. The methods so far, required large field data collection which is either not accessible or there is lack of compatibility by methodological changes. Traditional measurements for ET estimation are at fixed time instances and regular (daily) intervals. Such measurements, however, are costly and time consuming. Moreover these measurements are related to specific site locations. Due to the changing climate and the dynamic behaviour of water-heat transfer, estimates cannot be interpolated or extrapolated in a large basin (Gao et al., 2008). In shallow groundwater modelling, simulation of evapotranspiration loss and its spatial distribution often is complex. Remote sensing methods are currently considered appropriate methods to obtain different parameters in the required spatial and temporal scales to estimate the evapotranspiration (Santos et al, 2009).

1.2. Problem statement

In areas with a shallow groundwater table, estimation of groundwater recharge by considering evapotranspiration is critical for sustainable water resources management. Traditional groundwater flow models often oversimplify the recharge and evapotranspiration fluxes by use of simple source and sink term approximations. However, these two factors have great variability based on topography, soil type, land use, time, space, and water management practices, making their estimation difficult.

Recharge is one of processes in groundwater modelling which varies over space and time and thus can be quite uncertain. Remote sensing based methods to directly evaluate recharge are not available. However, RS and GIS methods can help to assess recharge indirectly (Lubczynski and Gurwin, 2005; Shaban, 2006). In spite of being difficult to quantify, it is necessary to estimate groundwater recharge in all forms to understand its impacts on local water extraction. The accurate estimation of the spatial distribution of the recharge is essential in producing reliable models. A large number of these models simulate water flow in the aquifer which can be calibrated for long-term behaviour modelling of any given aquifer using different management scenarios.

Clearly, for groundwater recharge assessment it is essential to have a detailed investigation on the impact of ET on the groundwater recharge. So far no detailed computation of ET in the Salland area has been done and the only data available is from generalizations of the nearby stations. By having access to the up-to-date satellite data with high spatio-temporal resolutions, this study aims to test and to use these data to quantitatively estimate the impact of ET on the groundwater behaviour. The main question of this study is: 'Could remote sensing based ET estimates contribute to improved recharge estimates in groundwater modelling in the Salland area in the Netherlands?'

1.3. Research Objective

The main objective of this study is to evaluate how recharge is affected when satellite based evapotranspiration is used instead of in-situ based evapotranspiration for the Salland study area, in the Netherlands. Specific objectives of this study are:

- To calculate recharge fluxes and hydraulic heads especially for the Salland area using in-situ based data
- To compare MIPWA-CAPSIM simulated ETa maps with SEBAL-based maps
- To analyse the effects of the different ETa estimates on recharge
- To tune root zone model parameters of the "Feddes" model approach
- To determine the water balance of the study area

1.4. Research Questions

- What is the sensitivity of the model to changes in CAPSIM parameters and time series of precipitation and evapotranspiration?
- What is the effect of changing actual evapotranspiration in Feddes equation?
- What is the result of modification of Feddes equation in recharge and hydraulic heads?
- Is there a significance difference in the calculated water balance components by using the in-situ based and SEBAL-based evapotranspiration?
- Are the calculated results obtained from the two approaches comparable?

2. LITERATURE REVIEW AND MIPWA DESCRIPTION

2.1. Recharge estimation and remote sensing

Recharge

The recharge concept is defined as downward water flow to the water table thus affecting the groundwater table. At the land surface precipitation water infiltrates the shallow soil layers but not all water reaches the water table so the net supply of water in a given area is less than the total amount of the water that is infiltrated.

Various sources of recharge have been identified in the groundwater system. Mechanisms that feed these resources were conceptually defined by Lerner et al. (1990) as follows:

- Direct recharge: remaining water after evapotranspiration and soil moisture, are added to the groundwater by direct infiltration through the vadose zone.
- Indirect recharge: Influence of surface water on groundwater flow through the bed.
- Localized recharge: an intermediate form of groundwater recharge resulting from the horizontal (near-) surface concentration of water in the absence of well-defined channels.

The required procedures in estimating recharge can be classified into three categories based on the hydrologic zone where the data was obtained (surface, unsaturated zone and saturated zone) (Scanlon et al. 2002). Estimation methodologies for each zone are: physical (direct and indirect measurements), tracer (use of artificial or naturally occurring chemicals) and numerical modelling (groundwater behaviour simulation). There are several recognized methods based on water-budget equation and the importance of directional flow in karstic systems. Methods were also classified by De Vries and Simmers (2002) as: direct measurements, water balance methods, Darcian approaches, tracer techniques, and empirical methods.

Remote sensing

Lillesand and Kiefer (2004) defined remote sensing as "acquiring information about an object, area or phenomenon by sensors with no contact with what is being investigated". According to this definition, space-borne and airborne data acquisition (in the visible, infrared, microwave and radio-wave, magnetic and gravity fields) as well as data acquired from near-surface about ground surface or subsurface by various geophysical techniques, can be categorized as remote sensing.

Digital Elevation Models, rainfall, evapotranspiration, land cover and snow cover are among the well-known remote sensing products that can be used in surface hydrology modelling (Schmugge et al., 2002). Remotely sensed data commonly is used in an indirectly fashion for numerical groundwater studies. Data often aims at linking and coupling of the surface runoff with groundwater models (e.g. Bauer et al., 2006). However, direct remote sensing applications in groundwater numerical modelling is limited due the low penetration depth of most of the sensor techniques.

Becker (2006) reviewed several remote sensing applications on acquiring quantitative data for groundwater studies and concluded that: "The best that can be achieved with satellite sensors is i) to determine spatial distribution of groundwater discharge and recharge areas, and ii) to assess storage changes over vast areas or measurement of surface water heads in large river bodies".

Brunner et al. (2007) showed specific applications of various well-known sensors, and concluded that the quantitative data on recharge and discharge distributions are the most useful remote sensing data for groundwater numerical modelling. Brunner et al. (2004) stated that the satellite-derived assessment of relative recharge can be achieved by rainfall and evapotranspiration data and comparing them with the recharge determined by the chloride method.

Remote sensing (RS) techniques can provides low cost spatio-temporal surface and subsurface information, both as the main data source for groundwater modelling as well as extrapolating tool for the data acquired by other methods. The ability to calculate ET without quantification of other complicated hydrological processes is considered as the primary advantage of these techniques. It makes it possible to compute the spatio-temporal evapotranspiration between two successive images which make it possible to model evapotranspiration as a highly variable parameter in both time and space. Variability in space is attributed to the variability of precipitation, hydraulic conditions of soils, and vegetation types and densities in different areas and its variability in time is due to variability of seasons and climate. Therefore, remote sensing imagery is considered as ideal powerful tools in determining and mapping the spatial and temporal structure of evapotranspiration.

Evapotranspiration

Evapotranspiration is one of the main water loss mechanisms in a watershed. Monitoring and evaluation of the changes in a given time period can be used to show the amount of water in each land use, and water management at the watershed scale can be achieved by determining the amount of water that can be allocated to each land use. Vast areas of natural resources and watersheds and the limitations in field studies by evapotranspiration recording stations, makes remote sensing an appropriate method in determining the actual evapotranspiration in different land use and watersheds. The calculation of evapotranspiration can be done experimentally using weighing lysimeters, Eddy correlation and Bowen ratio techniques. However, these methods are limited, since they provide point values of evapotranspiration for a specific location and fail to provide evapotranspiration values on a regional scale. This limitation has motivated the development of using remotely sensed data from satellites to evaluate evapotranspiration over vast areas.

The processes of water uptake by plants roots have been an interesting issue to study among the scientist in biology, agriculture, soil physics and environment. Several people have tried to model this phenomenon and used the actual farmland and laboratory data to evaluate and validate their models. The evaluation of water absorption by roots is of significant importance in hydrologic and even climatologic models. Also hydrologic and vegetation models require a quantitative analysis of the amount of uptake water (Feddes and Raats 2004, Kleidon and Heimann 1998). Feddes (1978) considered equal water absorption patterns for different depths, while, Prasad (1988) considered it linearly declining by depth.

Empirical macro-models estimate the amount of water exit from the root zone of soil as a whole and do not consider roots absorptions individually. Several studies worldwide have shown good results of this method when compared to actual farmland conditions. The basis of macro-models was the suggestion of Molz and Ramson (1970-1971) in which the water absorption by root was considered as the actual plant transpiration.

Evapotranspiration in water balance studies is generally studied by two methods. First, calculating the evapotranspiration as a passive component in the water balance equation after calculation of the sum of other components and subtracting it from the total water balance. In the second method, by direct or indirect methods (computational) component of the water balance equation can be calculated.

Most of the developed models to estimate ET from remote sensing imagery have been used in agricultural areas. Developments in modelling and remote sensing technology were used to determined distributed spatial data for certain parameters such as: evapotranspiration (Bastiaanssen et al., 1998), rainfall (Milewski et al., 2009), and soil moisture (Chabrillat et al., 2002; Ben-Dor et al., 2004).

Kampf & Tyler (2006) and Bastiaansen et al. (1998), employed multispectral satellite imagery and surface energy balance modelling to estimate ET. The Surface Energy Balance Algorithm for Land (SEBAL) algorithm is one of the cases that come to the aid of remote sensing in order to calculate the actual evapotranspiration rate. It is used to model the actual evapotranspiration using satellite based images. The algorithm was developed by Bastiaanssen (1998) and is based on the energy balance equation.

Modelling

A large number of groundwater studies rely on numerical modelling by use of MODFLOW which is a computer program that numerically solves the three-dimensional groundwater flow equation for a porous medium using a finite-difference method (McDonald and Harbaugh, 1988). Evapotranspiration is one of the input data of the MODFLOW model which is used for groundwater modelling in a catchment. Various algorithms and models have been developed to estimate evapotranspiration over larger scales combining remote sensing data and meteorological data.

Recharge is one of data types in groundwater modelling that has an uncertain nature. No remote sensing based method has yet been developed evaluate recharge directly. However, RS and GIS methods can help to assess recharge indirectly by using GIS modelling to scale up recharge estimates with other methods (Lubczynski and Gurwin, 2005; Shaban, 2006). Moreover by assessing P and ET and spatial mapping of them, RS can be used to scale up chloride based recharge estimates (Brunner et al., 2004). By using recharge measurements as the model reference, remote sensing can be employed in stochastic modelling of P-ET (Hendrics-Franssen, 2006).

To define the space-time distribution of groundwater recharge, Khalaf and Donoghue (2011) applied geospatial techniques in conjunction with groundwater modelling. Hydrogeological data in a GIS format were combined with the data derived from satellite images (land cover, evapotranspiration, precipitation, and DEM derivation) to identify and map the key surface indicators of recharge areas for each pixel.

E. Pardo-Igúzquiza et al. (2012) used a distributed approach both in time (daily estimates) and in space (a raster cell model) to estimate recharge in a karstic mountain regions. Their method included the most significant components of recharge in water budget (i.e. rainfall and evapotranspiration) and excluded the components (vegetation interception and ponding) that have values within the error range of major components. Daily water budget was calculated for each cell.

2.2. Groundwater modelling

There are a number of definitions for a model, for modelling and for simulation. A model simulates spatial and temporal properties of a system or some of its components physically (actual) or mathematically (abstract). Using the model and controlling its output results is called simulation. Every tool which provides an estimation of field conditions is called a "model". Groundwater models are often used in the evaluation of water resources and determination of the conditions of long term water exploitations from aquifers in regional or local scales. Flow model in particular can provide useful information on hydraulic parameters such as flow rate, water table withdrawal and flow direction. Moreover, underground conditions are not easily accessible or observable thus making models practical tools to understand and simulate groundwater systems and predict their behaviour. Groundwater simulation models are classified into physical, analogue and mathematical (empirical, probabilistic, and causal) models.

2.2.1. Mathematical models

Models in which the groundwater flow components are described by mathematical equations are called mathematical models. Mathematical models can be solved analytically or numerically. Simple Darcy or Laplace equations can be used in definitive mathematical models.

Numerical models describe the whole flow field simultaneously provided that there exist a mathematical solution for each user designated point. In these models, the area is divided into several smaller areas known as "cells". The basic flow equation is solved for each cell considering its water balance. Numerical model results in the determination of hydraulic head in designated points in each individual cell. These points can be chosen in the centre of each cell or the intersection of adjacent cells or any other point in the cell. Differential equation for ground water flow is an algebraic equation with n equations with n unknowns in which n denote the number of cells. The algebraic set of equations (matrix equation) is solved numerically by iterations, hence the name numerical models. The finite differences (FD) approximation is the most common numerical method in groundwater modelling.

Governing equations of groundwater flow are based on Darcy law (1856) that is generalized in 3 dimensions and the continuity equation. Certain assumptions of the system to be simulated are expressed and imposed by Jacob's equation (1950), Laplace equation and Dupuit-Forshheimer assumptions.

2.3. MIPWA model

2.3.1. Introduction

The project 'Development of a Methodology for Interactive Planning for Water Management' (MIPWA) was established in 2005 to address various and often conflicting interests of water management entities. Some 17 water management parties including water companies, water boards, provincial water management organizations and municipalities joined the initiative to develop a large-scale high-resolution decision support tools to address groundwater-related issues. MIPWA includes a groundwater model for the northern part of the Netherlands with 25m × 25m spatial resolution; an emergency response database on intervention needs which provides different scenarios that can be

explored by decision making bodies. It uses an internet accessible user-interface facilitating access to model data for related managers (after Berendrecht et al 2007).

The MIPWA project area is shown in Figure 2-1. The area mainly consists of various agricultural and natural resource areas with small amount of urban development. Some 50 percent of the area has elevations close to the sea level and is characterised by dispersed small water channels mainly controlled by weirs and pumps. The rest of the area has a gently sloping drainage system facing north-west. Approximately 380 million m^3 per year is withdrawn from groundwater resources to provide for drinking water and industrial demands.

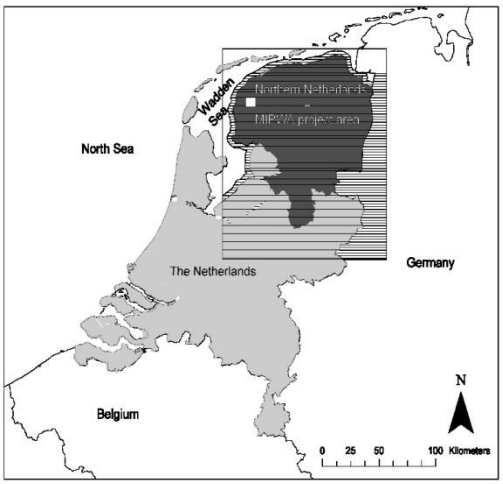

Figure 2-1, MIPWA project area (dark grey) and the total modelled area (shaded) (Berendrecht et al, 2007)

2.3.2. Model-Contraction Process

Different geographic settings and the water management challenges require a detailed groundwater model on a regional scale capable of addressing various groundwater issues. Spatial planning and water management is the main focus of the MIPWA model and it can be extended to other management issues in future. Both steady state and transient flow conditions can be simulated by this model by adapting specific numerical boundary conditions. Effects of numerical boundary conditions were reduced by using a buffer zone around the study area (145 km East-West and 167 km North-South).

The MIPWA model is based on the MODFLOW (McDonald and Harbaugh, 1988) model with spatial resolution of 25m×25m making a total of 238.000.000 model cells (Figure 2-1) distributed over seven layers. In non-steady state simulations it applies time step of 1 day. Prior to this study, model runs are available for the 1989-2001. Due to their high influence on planning, shallow groundwater processes were given high priority (Figure 2-2) and the coupled MODFLOW–SIMGRO code was used to model the unsaturated zone (Veldhuizen et al., 2006).

An Interactive modelling interface iMOD is available which allowed the storage of model inputs and results on a server (Vermeulen et al., 2006).

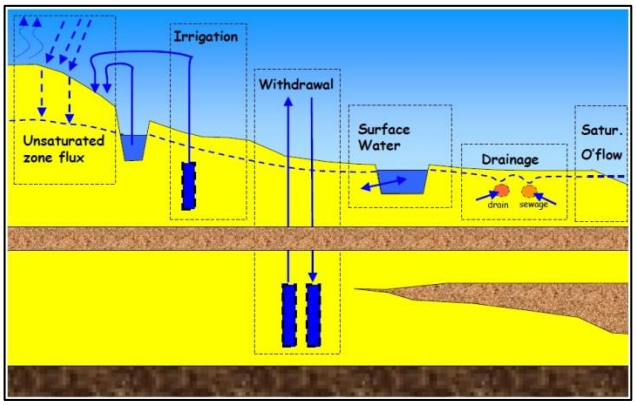

Figure 2-2, Processes described by the MODFLOW-SIMGRO model (Berendrecht et al, 2007)

2.3.3. iMOD Definition

iMOD stands for Interactive MODeling which is a user-friendly interface (iMOD and iMODFLOW) to support the use of (large-scale) groundwater flow models, based on the concept of MODFLOW. iMOD is specially designed to handle large models that are not supported by commercial GUIs, such as GMS and Visual MODFLOW.

iMODs philosophy is to construct large scale input files for a variety of parameters that are needed for a groundwater flow model. Instead of focussing on a local area for which a local study needs to be carried out, data is collected for a large area. Within this large area, other local models may be constructed in the near future. Therefore, since various models can be constructed with different grid sizes with local grid refinements, the applicability of the model increases.

Another simplification compared to the commercial packages is that iMOD uses iMODLOW, restricting the number of different input formats drastically to maximal 4, with one format covering about 90% of all input- and output parameters.

The main functionalities of iMOD are:

- Visualizing and analysing model input and output, e.g. 2-Dimensions plots, time series, cross-section, 3-Dimensions analysis, water balancing
- Starting a groundwater flow simulation, flow paths
- Generation of scenarios
- GIS functionalities, e.g. raster manipulations, plotting.

Most of the iMOD functionalities are tailor-made for customers, such as the water balance tool, the 3D-tool and flow path simulation. Efforts to improve iMOD are (still) ongoing. iMODFLOW directly relates and links to the concept of MODFLOW (USGS). However, to perform optimally in relation to large extraordinary simulation models, the input-output (IO) structure is altered such, that it can process raster files at different orientation and resolution. Furthermore, the input files for the most important packages are unified to raster, line and/or point wise data, to be visualized directly within iMOD accordingly.

2.3.4. Files

The following file formats are used within iMOD:
*.PRF, *.IMF, *.IDF, *.MDF, *.IPF, *.IFF, *.ISG, *.GEN, *.DAT, *.ASC, *.LEG, *.CLR, *.DLF, *.CRD, etc. Detailed explanation of these file formats can be found in Appendix 1.

2.3.5. Runfile

To initiate a groundwater flow model simulation using iMODFLOW, a Runfile is required. This file describes:
- The location and model domain area of the (sub) model
- The simulation period and the stress periods for model forcing
- The distribution of computational nodes (grid size) and spatial resolution
- The number of model layers to be used in the modelling
- The collection of files that describe the model parameters and other inputs
- The desired output variables to be saved

A Runfile gives an overview of the (entire) model configuration, making the model easy to apply to selected areas and to simulate specific time periods and field conditions. A major difference between the input files necessary for standard MODFLOW approaches is that the Runfile does not contain any model data but essentially is a batch file. It mainly redirects to files (IDFs, IPFs, ISGs, GENs) that contain the actual model data.

The philosophy of using iMODFLOW and the concept of a Runfile is that all the referred files are constructed for a region of interest rather than for a specific area of interest. A region of interest can be extremely large; an area of interest is often smaller. The key-thought is that model data is collected for large regional areas at the finest spatial scale available for that type of model data, e.g. land use observations at a resolution of 100m x 100m and precipitation distribution at a scale of 1000m × 1000m. These files are referred to in a Runfile and iMOD combines the different data to the desired AREA of interest and resolution at the moment a simulation starts, (see Figure 2-3).

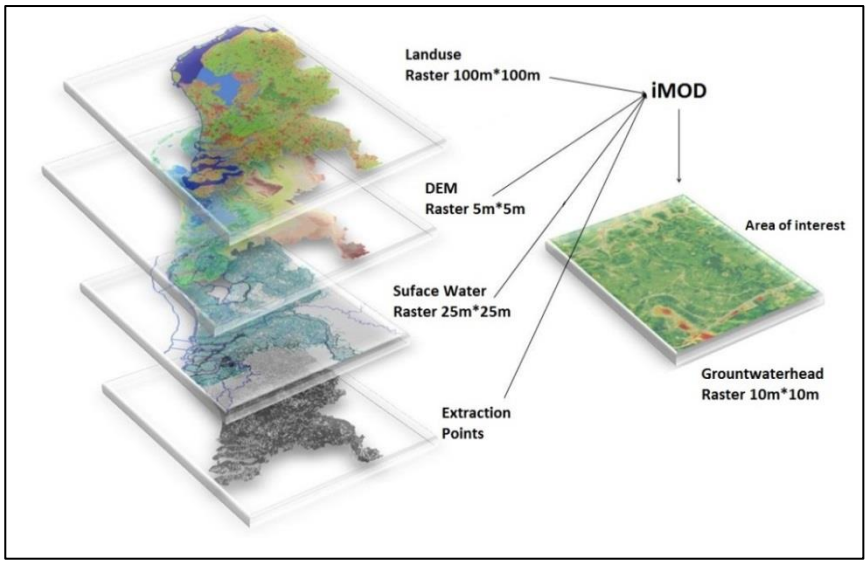

Figure 2-3, Concept of iMOD processing

2.4. CAPSIM part of MIPWA model

For simulation of the unsaturated zone and related processes such as e.g. actual evapotranspiration, recharge and infiltration, the CAPSIM model was coupled to the MIPWA model. The main objective of coupling was to improve recharge estimation to the MIPWA model by an unsaturated zone flow model that relies on accurate simulation of precipitation inputs and evapotranspiration losses to better asses recharge fluxes in time-space domains. Groundwater recharge and discharge are exchange fluxes between groundwater table and the unsaturated zone and streams. To determine the groundwater recharge, CAPSIM model is coupled to the MIPWA model. The concept of groundwater recharge process is shown below in Figure 2-4.

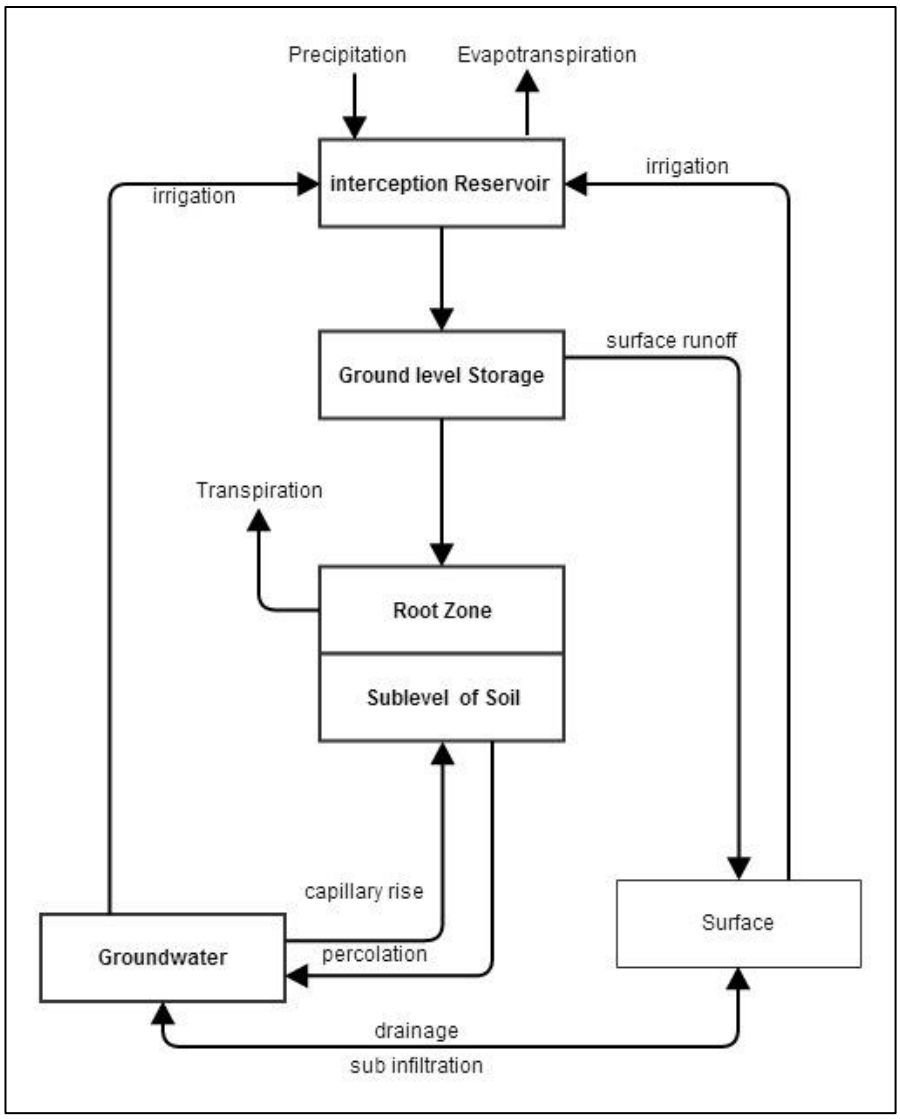

Figure 2-4, CAPSIM component of MIPWA model

The driving force behind the groundwater recharge is net precipitation that is affected by precipitation, evapotranspiration and soil water storage in the unsaturated zone. Net precipitation is defined as the precipitation amount that contributes to the ground water storage. In the CAPSIM model, precipitation on the vegetation is intercepted of which a part is evaporated to return back to the atmosphere. Conceptually, vegetation is considered an interception reservoir which usually

overflows quickly. The water that reaches the soil is either infiltrated or discharged as overland flow when infiltration capacity is limited. Overland flow as caused by high precipitation rates is ignored in the CAPSIM model.

The water infiltrates the top layer of the soil. The unsaturated zone is the zone from which the vegetation can extract water with their roots and thus serves the evapotranspiration directly. This zone is called the root zone which is also considered a water storage reservoir. Like all other reservoirs, this reservoir has a maximum storage capacity. If exceeded the excess water leaves the reservoir, e.g., by recharge. In the model approach, capillary rise is partly dependent on the groundwater table where high groundwater tables may result in high capillary rise. The storage of the unsaturated zone is also dependent on the groundwater. Large water storage in the unsaturated zone triggers down ward flow and thus affects recharge. This causes water storage in the saturated zone and causes rise of groundwater levels. The MIPWSA-CAPSIM approach is used to model the above mentioned processes.

3. STUDY AREA

3.1. Study Area

The water management area of Groot Salland Water board is located in the western part of the province of Overijssel, in the Netherlands (Figure 3-1). The boundary of this management area is broadly based on (sub)-basins. The Water board itself is part of the Vecht/Zwarte water catchment, which is part of the Rhine Valley. The size of the management area is approximately 120,000 acres, in which the water board manages over 4,000 kilometres of water courses. The management area has population of approximately 360,000 and hosts a large number of companies. (The informations have been adapted from Waterschap Groot Salland website: www.wgs.nl).

The Nationaal Park Sallandse Heuvelrug is the south-east boundary of the area. The north-east of the area is bounded by open water which is called "Zwarte Meer". The municipalities Dalfsen, Deventer, Kampen, Olst-Wijhe, Raalte, Staphorst, Zwarte Waterland and Zwolle are located within the boundaries of this water management area. Small parts of municipalities Hardenberg, Hellendoorn, Ommen and Rijssen-Holten are also located within the area (Figure 3-2).

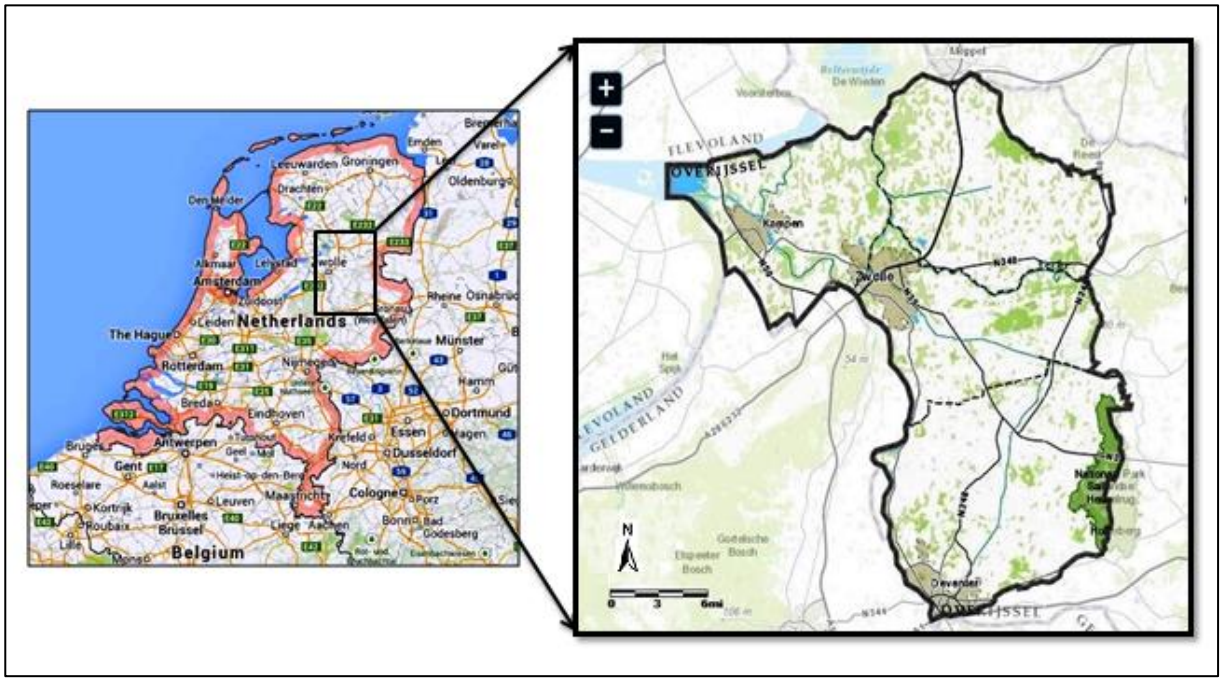

Figure 3-1, Location of Groot Salland in the Netherlands (Black boundary)

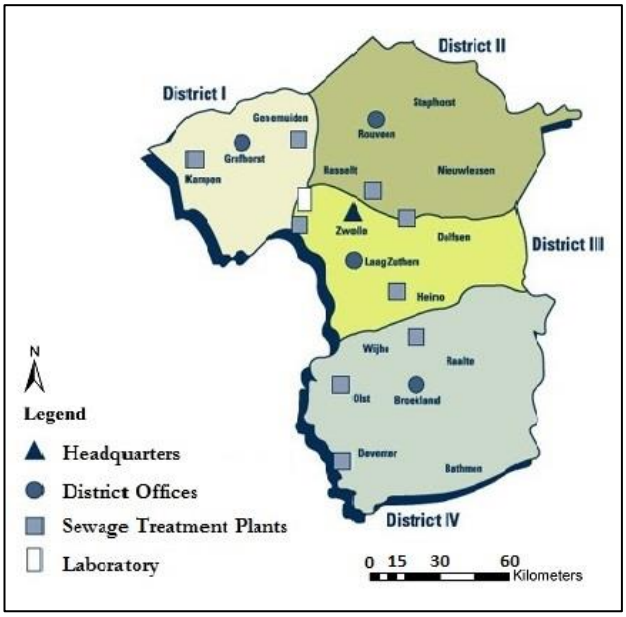

Figure 3-2, Management of study area (www.wgs.nl)

3.2. Area description

The areas of the River Rhine water boards include central-eastern and south-Drenthe, Overijssel, the border, and the southern part of the Veluwe. The IJssel is the western border of the area. The joint management area runs from east to west. Therefore waters from all the individual parts ultimately flow to the IJssel and the Zwarte Meer. The lowest point in the area is 2 meters below sea level which is located in the northwest and the highest point with more than 60 meters of elevation is located in the southeast (Figure 3-3).

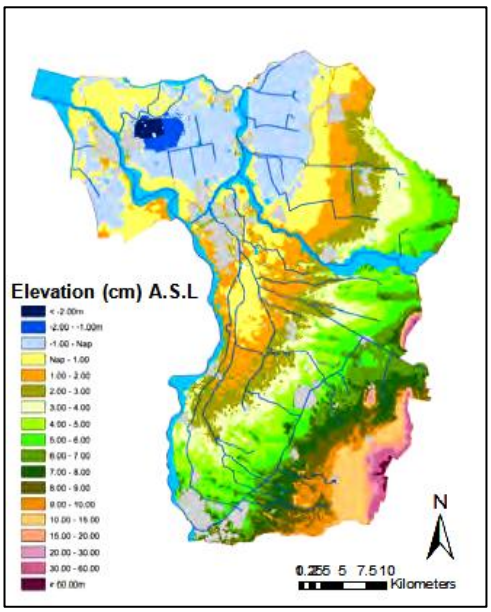

Figure 3-3, Digital elevation map of the study area

3.3. Distribution of Soil type

Based on geomorphology and soil type, five types of landscapes and regions can be distinguished. The moraines (Overijsselse Heuvelrug) consist of coarse gravel and sandy deposits to a maximum height of 70 m ASL. Mostly wooded, but some large moors have been preserved. There is no open water present, and the groundwater is deep.

As shown in Figure 3-4, sandy soils are most abundant in the area. Western and north-western parts of the area are covered with clay. The north of Zwolle and a part of the west of the study area is covered with peatlands.

The gently sloping Aeolian deposits (The eastern half of the management area) consists of a number of fairly flat plateaus covered with layers of loess sand and alternating parallel layers spread over sand ridges and hollows. Near the river IJssel (in the west) these deposits were later covered with clayey fluvial deposits. The area consists mainly of grassland with some local woods and heathland remnants. In some areas, park-like landscapes occur with estates and historical sites and the ground level is gently inclined from the southeast to the northwest.

The fluvial area, along the IJssel and Vecht rivers in the east and center, consists of sandy levees, river dunes near the river and further away from clayey hinterlands. At the transition from river to wind deposits are mixed soils and the landscape consists of arable land and grassland.

The lower layer of the vast, flat and open peatland consists of peat and wedges of blown sand. Several long narrow plots are separated by ditches. In inland areas (near Zwolle) the bog is preserved and covered with a layer of clay. Peat and marine clay areas are mostly covered with grassland. (see Figure 3-4) (These informations have been taken from Waterschap Groot Salland report: WATERBEHEERPLAN 2010-2015).

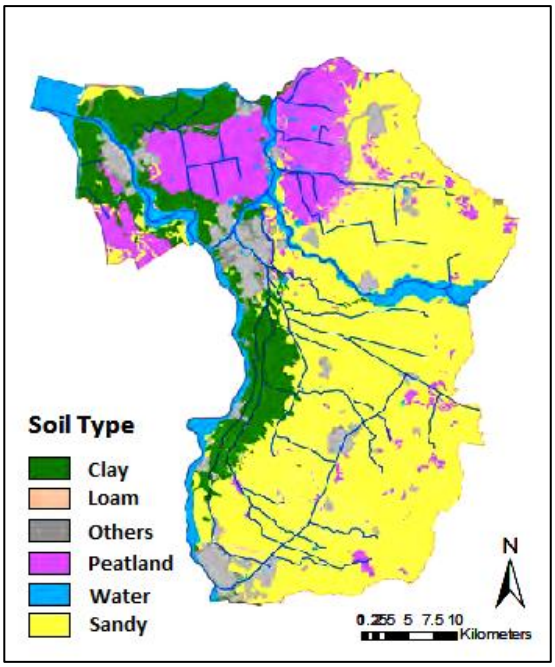

Figure 3-4, Distribution of Soil type map of Salland area

3.4. Geo-hydrological parameters and system representation

The aquifers and 7 separating layers (i.e., aquitards) which are defined in the schematization during the initial parameterization feature hydro-geological parameters. (Figure 3-5). Aquifers are parameterized by a kD value (Transmissivity) [m²/day] to reflect on layer transmission capacity. Each of the 7 separating layers is parameterized by a c-value [days] to reflect on hydraulic resistance toward vertical flow. Initially, the parameter values are assigned based on horizontal permeability Kh (known as Regis sand and complex layers) and vertical permeability Kv (known as Regis clay, peat and complex layers) (Figure 3-6). For the upper layer, kD and c-values are assigned for the freatic (sand) and sealing (clay) layer, respectively, and therefore can be calculated separately based on the characterization of the land which covers top system (Van der Linden, 2002).

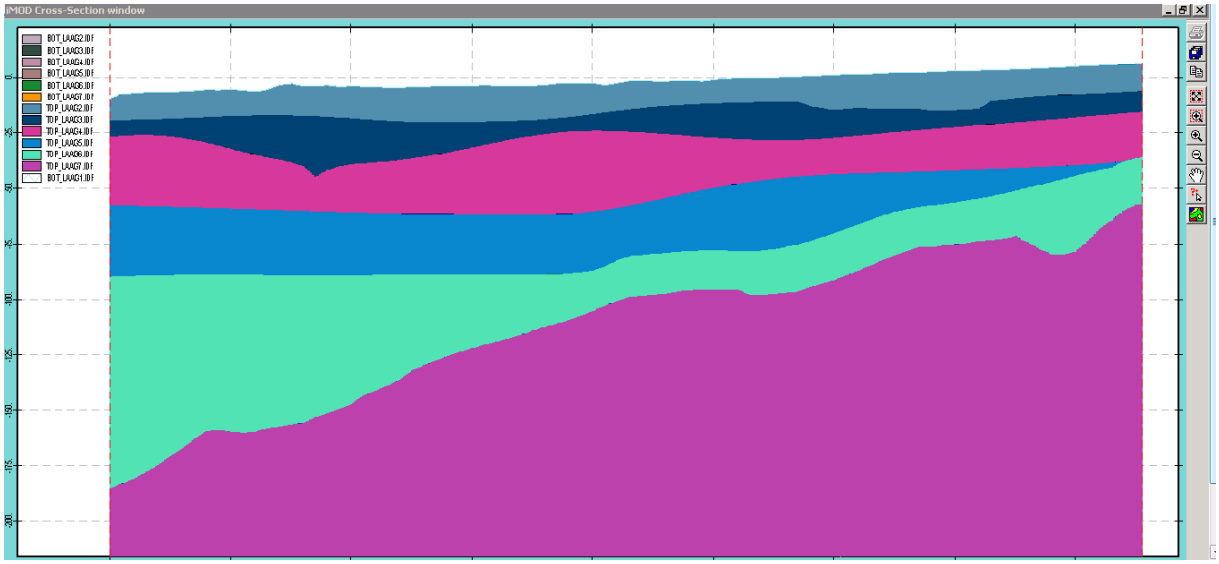

Figure 3-5, Cross-section of 7 separating geologic layers.

Regarding the layer maps in figure 3-6, the first three layers have the smallest transmissivity values; whereas the 7th layer has the largest. It seems that the lowers layers are suitable and appropriate for groundwater extraction purposes due to their large hydrodynamic storage coefficients. High c-values limit groundwater flow movement from one layer to another one (C3 and C6). In fact, the groundwater flow movement will be slow and obstructed due to large c-values; whereas the low c-values allow more groundwater flow between two layers (C1, C2, C4 and C5).

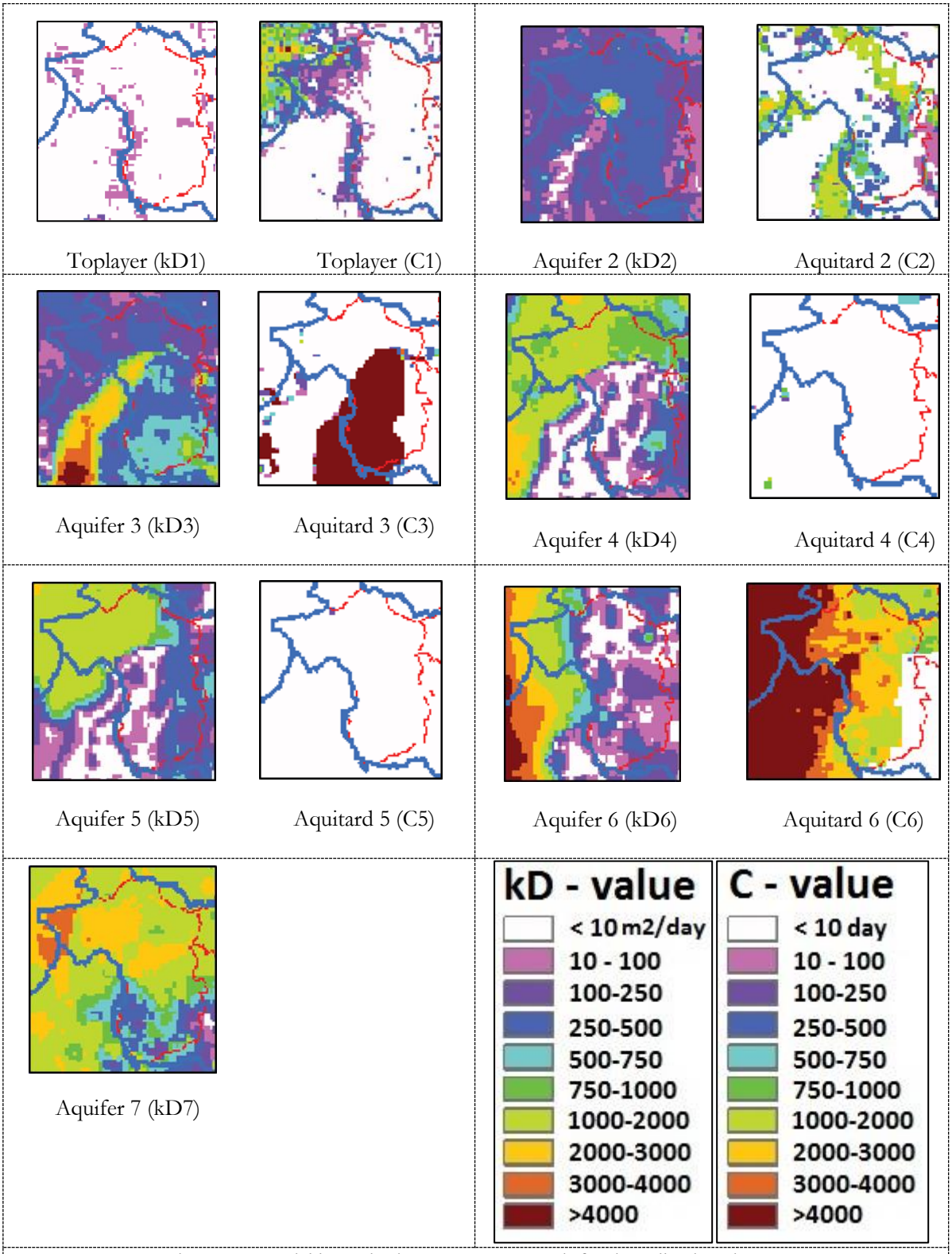

Figure 3-6, Model layers in the MIPWA approach for the Salland study area

4. DATA COLLECTION

4.1. CAPSIM

The MIPWA-CAPSIM model used for this study is the operational model prepared by the Salland Water board. All soil data, subsurface data and meteorological data for the area is prepared in a data base and entered to the model. For running the model, all data is accessed through a run file as described above.

The amount of recharge is estimated for each cell in the MIPWA-CAPSIM model and therefore the following characteristics of the region should be known:

- Precipitation
- Evaporation
- Land use
- Soil physical unit
- Infiltration capacity of the soil
- Root zone thickness.

The following seven text files are required for running the CAPSIM model.

FACT_SIM: Crop factor
FILT_SIM: Soil physical and infiltration capacity
LUSE_SIM: Land use
PARA_SIM: Start and stop day number for calculations
ROOT_SIM: Root zone thickness and relative root zone storage
UNSA_SIM: Soil physical unit number, thickness of root zone and depth of groundwater below soil surface, storage of root zone for drying/ wetting conditions and capillary rise flux

Based on the generated run-files for the CAPSIM model, seven other text files are required. After the compilation of the run-file, four of them are created with constants (i.e. fixed values) for each cell as follows:
AREA_NOD: Land use and thickness of root zone
COND_NOD: Layer number, layer thickness, specific storativity per meter layer thickness (i.e, storage coefficient) and hydraulic conductivity
GIFT_NOD: Abstraction from surface water and groundwater
NODE_SIM: External node number and soil surface above mean sea level and (x-coordinate, y-coordinate)

The last two files which should be completed by data collection are related to the time period of the study:
TIME_SIM: is the set up for time steps
MIPWA model was run for 1989-2001 period till now. Since our in-situ data cover the period 01-05-2012 to 01-05-2013 period input time series were reset to cove for the 01-05-1999 (replace of 2012 dates) – 01-05- 2000 (replace of 2013 dates) were defined in the 'TIME_SIM' file.

METE_SIM: is the input file for precipitation and evapotranspiration for all of the stations in the study area.

4.2. Precipitation

For the simulation period, time series with daily sums of precipitation and evaporation were used. Figure 4-1 shows the precipitation stations that are used in this thesis study. Precipitation data are collected from 01 May 2012 to 30 April 2013 from KNMI website for the stations marked in white.

Table 4-1 shows names and numbers of the KNMI precipitation stations in Figure 4-1. The specified 24-hour precipitation was measured from 08:00 UTC on the previous day to 08:00 UTC on the date indicated. The precipitation data are available at daily base and precipitation depth is displayed in tenths of millimetres.

Table 4-1, Names and numbers of the KNMI precipitation stations

	Name	Number
1	Heerde	328
2	Zwolle	330
3	Ijsselmuiden	335
4	Heino	340
5	Vilsteren	342
6	Nagele	352
7	Dedemsvaart	354
8	Rouveen	358
9	Dronten	364
10	Epe	514
11	Hellendoorn	672
12	Lettele	681

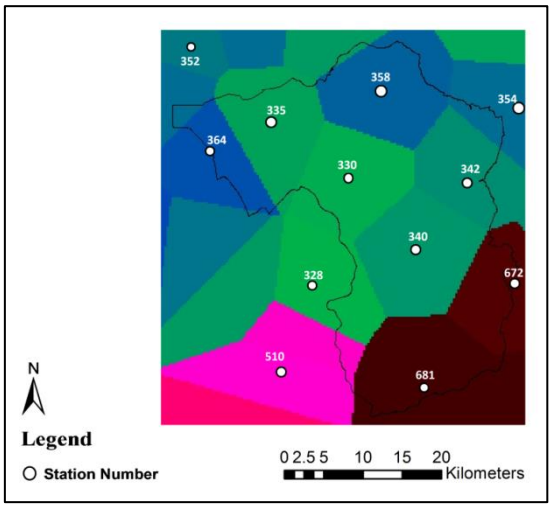

Figure 4-1, Thiessen polygon of KNMI meteorological stations

The measured precipitation of station "Zwolle_330" for each month is shown in Figure 4-2.

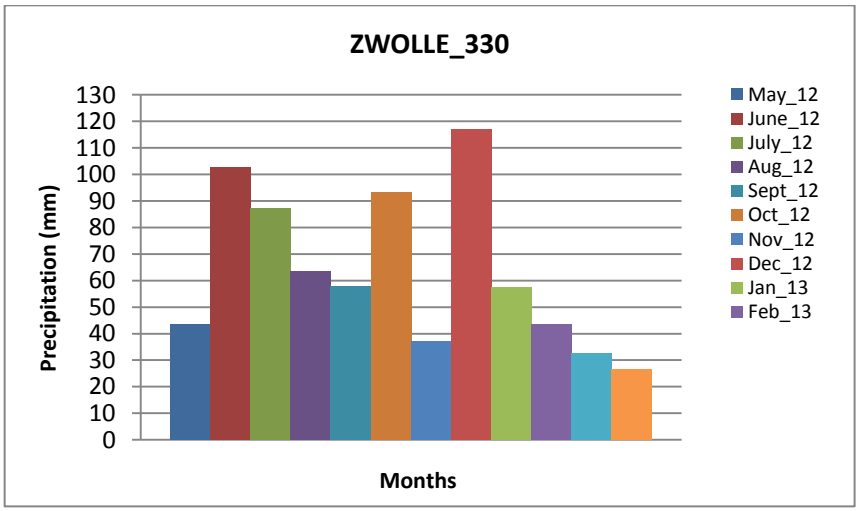

Figure 4-2, Precipitation of Zwolle station

4.3. Evaporation

Since there is too little data available for calculation of Makkink evaporation in the study area, data from two Metadata KNMI stations, (Figure 4-3 and 4-4) were taken for 01 May 2012 to 30 April 2013 period. The available data from the nearest stations in the north of the area (06273 Marknesse) was used for stations 335, 352, 358, 364 and the nearest station in the southeast of the area (06278 Heino) was used to replace data for the stations 328, 330, 340, 342, 354, 514, 672, 681.

Evaporation is a combination of plant evaporation and the evaporation of bare ground. According to the method used by Makkink (1957) for estimating evapotranspiration, there is no distinction between soil evaporation and crop transpiration. In the CAPSIM input file for precipitation and evapotranspiration (mete-sim), four ET classes are identified. In addition to the potential reference evapotranspiration which is received from two meteorological stations, three other data types are required which were calculated using the reference evapotranspiration coefficient. The potential evapotranspiration was multiplied a crop coefficient in order to estimate the pine forest and deciduous forest potential evapotranspiration. Also the constant evaporation (0.75 mm/day) is used for all the bare soil area. Crop factors necessary for calculation of evapotranspiration are shown in the Table, 4-2.

Table 4-2, Crop factors

Description	Crop factors
Potential evapotranspiration of pine forest	1.2
Potential evapotranspiration of deciduous forest	1.05

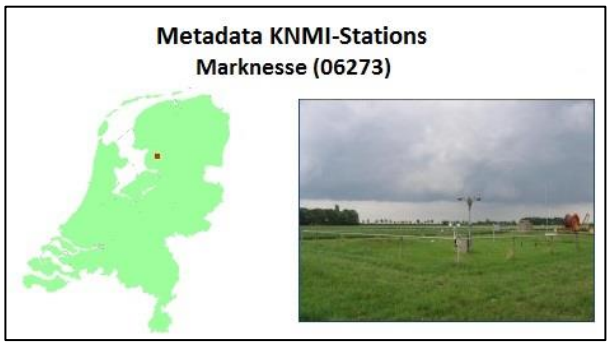

Figure 4-3, Location of Marknesse station

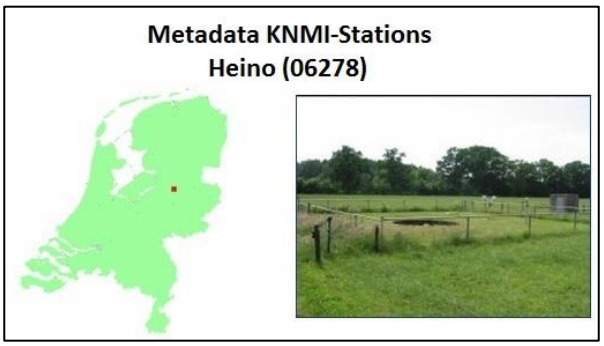

Figure 4-4, Location of Heino station

Table 4-3, KNMI stations information

	Station	Location	Terrain Elevation	Characteristic environment	Soil	Precipitation Measurements	Radiation Measurements
273	Marknesse	52° 42' N 05° 53' OL	(-) 3.35 M	Located in flat open polder mainly farmland Pasture	Clay	Electrical Measurements (English style)	CM11 sensor Measure height 2 m
278	Heino	52°26'N 06°16'E	+3.6 M		Sand	Electrical Measurements (English style)	CM11 sensor Measure height 1.5 m

The potential evaporation is the maximum evaporation and is independent on the availability of moisture in the root zone. To estimate actual evapotranspiration the Feddes method (1978) is used in part of the CAPSIM model. In the method, the so-called Feddes function serves for calculating the decrease in actual evaporation as a function of the pressure head (h) in the root zone and potential evapotranspiration (ETp). The latter is available for the simulation period based on time series with daily sums of reference evaporation according to Makkink.

The evaporation reduction is determined by the Feddes functions. Feddes et al, (1978) presented a simple term for reduction of water absorption to convert the actual transpiration as a function of pressure head in soil matrix:

$$S = \alpha(h)\frac{T_a}{Z_r} \quad \text{(Eq. 4-1)}$$

$$\alpha(h) = \frac{S(h)}{S_{max}} \quad \text{(Eq. 4-2)}$$

$$S_{max} = \frac{T_p}{Z_r} \quad \text{(Eq. 4-3)}$$

Where: S is root water uptake, S_{max} is maximum root water uptake, T_a is Actual transpiration rate [mm/day], T_p is Potential transpiration rate [mm/day], Z_r is Height of roots [mm], h is pressure head [mm], and $\alpha(h)$ is Reduction coefficient for root water uptake.

$$S = S(h)\frac{T_a}{T_p} \quad \text{(Eq. 4-4)}$$

The actual amount of transpiration can be considered equal to the absorption of water by root when there is no limitation of water availability in the soil. The absorbed water by the plant is equal to the potential transpiration.

$$S = S_{max} = \frac{T_a}{Z_r} \quad \text{(Eq. 4-5)}$$

If the soil cannot provide the plant water demand for maximum transpiration, $\alpha(h)$ serves to reduce from the maximum transpiration amount:

$$S = \alpha(h)S_{max} = \alpha(h)\frac{T_a}{Z_r} \quad \text{(Eq. 4-6)}$$

$\alpha(h)$ Is a function of soil suction is the ratio of actual water absorption to the absorption in ideal moisture conditions. Based on the existing suction in soil, they presented the following equation:

$$S = 0 \qquad h_1 \le h \le 0$$

$$S = S_{max} \qquad h_3 \le h \le h_2$$

$$S = S_{max}\left[\frac{h - h_4}{h_3 - h_4}\right] \qquad h_4 \le h \le h_3$$

$$S = 0 \qquad h \le h_4$$

Plants cannot absorb water when the pressure head (h) is between 0 to h_1 due to the lack of oxygen in the soil. In the second part; between h_1 to h_2; the absorption is maximum with reference to the suitable conditions for absorbing water by plant. In the third part; between h_2 to h_3; due to high suction in the soil, the absorption is gradually decreased. When the pressure head (h) is greater than h_3 then the plant cannot absorb any water. As the amount of suction reaches a threshold value of h_3, the actual transpiration linearly decreases in the model. The h_3 suction range is a threshold value for the plant in which the more transpiration, the more positive the threshold occurs. (See Figure 4-5).

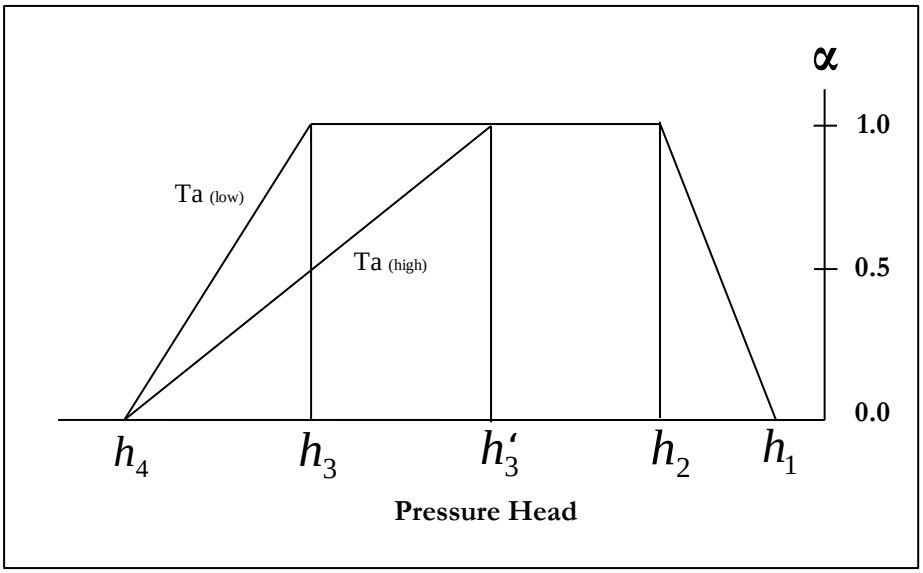

Figure 4-5, The reducing function of water absorption by plants in different matrix suction conditions

4.4. Actual Evapotranspiration

Several methodologies and sensors have been used for estimation of evapotranspiration in a regional and even global scale. SEBAL is a remote sensing algorithm for computing evapotranspiration based on instantaneous energy balance at pixel scale. The accuracy of representing the true actual evapotranspiration is reported at 85% for single days for an area as larger as 100 hectare. Bastiaanssen et al. (1998a,b) described that accuracy of this algorithm in a complete season can be increased up to 95%. For large watersheds accuracy is assumed to be 96% of the true actual evapotranspiration.

For this study, maps of actual ET as based on the SEBAL approach were available for the Salland region. The maps are available from 01 May 2012 to 30 April 2013 period with the exception of 12 December 2012 to 1 March 2013 in which the data is missing due to the unfavourable atmospheric conditions in winter Figures 4-6 and 4-7 show two samples of actual ET maps for 14st and 28th of May 2012.

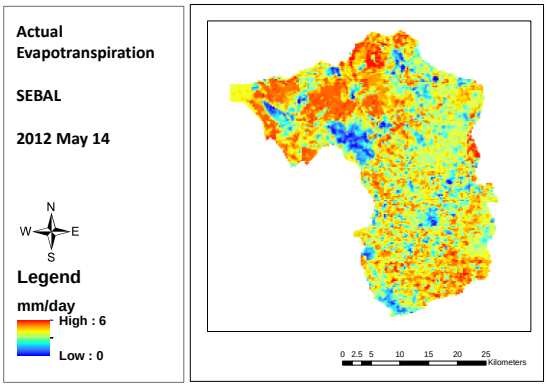

Figure 4-6, Daily SEBAL-based ETa map for 14st of May 2012

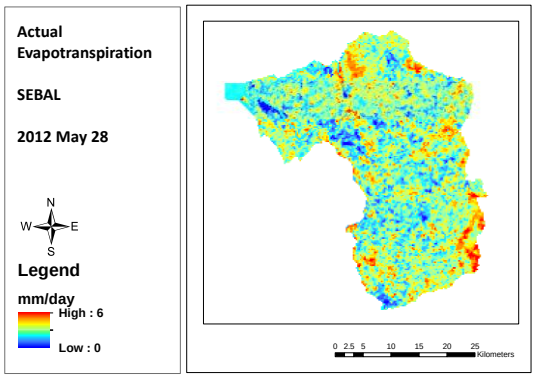

Figure 4-7, Daily SEBAL-based ETa map for 28st of May 2012

5. METHODOLOGY

Figure 5-1 shows an overview of the methodology applied in this study. After data collection and at the end of model processing, the model provides a map of annual cumulative ETa. In this step, the cumulative map is compared with SEBAL-based ETa maps.

If maps are not comparable, the expected outputs of the model will be re-evaluated. If the maps are comparable, then based on Feddes equation, the ratio between the two ETa maps can be applied as a coefficient in the root zone thickness value. After optimizing the root zone parameter, the model is run again. After the repeated run, new hydraulic head, water balance and recharge values are obtained as output.

In the last step, the model outputs before and after optimization are compared and finally conclusions and recommendations are presented.

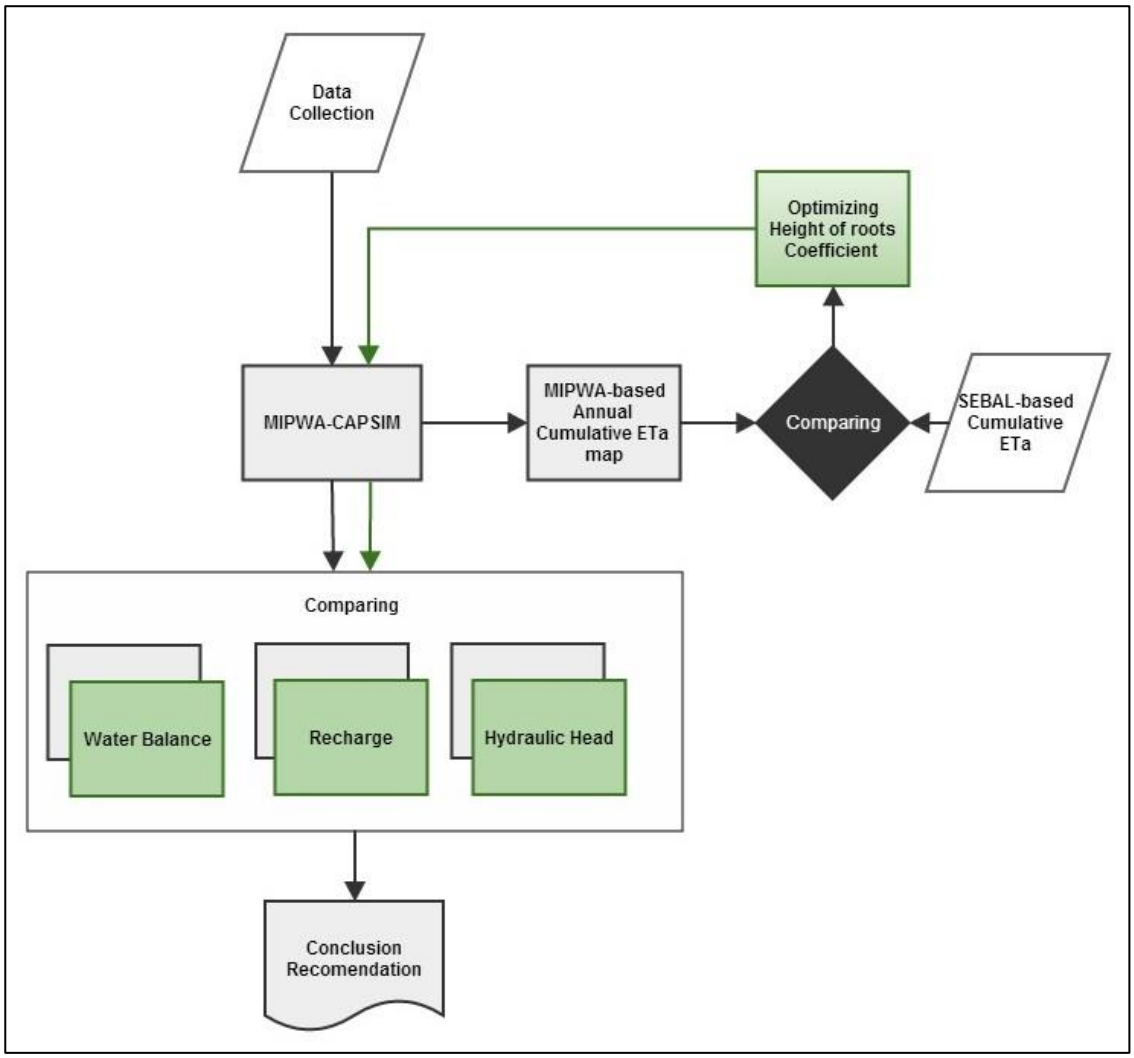

Figure 5-1, Methodology flow chart

5.1. Groundwater flow equation

Groundwater flow conforms to the fundamental hydrodynamic equation of porous media. In this section, empirical formula of Darcy and the law of mass conservation are used to express the flow equation in the porous media. A numerical solution often is based on the finite difference method in MODFLOW model. Based on the law of mass conservation:

Volume difference of stored water in the cell = The amount of water inflow – outflow

Based on Darcy equation, the amount of inflow and outflow is calculated as follows:

$$Q = kA\frac{h1-h2}{L} \rightarrow q = \frac{Q}{A} = k\frac{h1-h2}{L} \quad \text{(Eq. 5-1)}$$

Where:
Q: The amount of flow [L^3/T],
A: The cross section area of flow [L^2],
K: Hydraulic conductivity [L/T],
L: The distance between the inflow and outflow cross sections [L],
q: Darcy velocity or net flow or flow per cross section unit [L/T]

In the 3-Dimensional system, hydraulic conductivity is expressed as*:* k_{xx}, k_{xy}, k_{xz}, k_{yx}, k_{yy}, k_{yz}, k_{zx}, k_{zy}, k_{zz}.
In this system:

$$K=\begin{bmatrix} k_{xx} & k_{xy} & k_{xz} \\ k_{yx} & k_{yy} & k_{yz} \\ k_{zx} & k_{yz} & k_{zz} \end{bmatrix} \quad \text{(Eq. 5-2)}$$

The amount of flow (i.e., Dacry flux) in each direction reads:

$$q_x=-k_x\frac{\partial h}{\partial x} \qquad q_y=-k_y\frac{\partial h}{\partial y} \qquad q_z=-k_z\frac{\partial h}{\partial z} \quad \text{(Eq. 5-3)}$$

k_x, k_y and k_z are the hydraulic conductivity in *x*, y and z axis directions and parallel to the principal axis of hydraulic conductivity [L/t].

If these values are substituted in the mass conservation equation, the groundwater flow equation reads:

$$\left(\left[(Q\rho)_{x+\Delta x} + (Q\rho)_{y+\Delta y} + (Q\rho)_{z+\Delta z}\right] - \left[(Q\rho)_x + (Q\rho)_y + (Q\rho)_{z+\Delta x\Delta y\Delta z}\right]\right)\times \Delta t + [(\alpha\rho)_{t+\Delta t} + (\alpha\rho)_t]\Delta x\Delta y\Delta z = 0 \quad \text{(Eq. 5-4)}$$

Where: ρ is density and α is porosity.

By dividing the above d equation to $\Delta x\Delta y\Delta z\Delta t$ and after simplifying we get:

$$-\frac{[(Q\rho)_{x+\Delta x}-(Q\rho)_x]}{\Delta x\Delta y\Delta z}-\frac{[(Q\rho)_{y+\Delta y}-(Q\rho)_y]}{\Delta x\Delta y\Delta z}-\frac{[(Q\rho)_{z+\Delta z}-(Q\rho)_z]}{\Delta x\Delta y\Delta z} \pm R = \frac{[(\alpha\rho)_{t+\Delta t}-(\alpha\rho)_t]}{\Delta t} \quad \text{(Eq. 5-5)}$$

Since the flow intensity is equal to:

$$q_x = \frac{Q_x}{\Delta x \Delta z} \qquad q_y = \frac{Q_z}{\Delta x \Delta y} \qquad q_z = \frac{Q_z}{\Delta y \Delta z} \tag{Eq. 5-6}$$

And by assuming $\Delta t, \Delta z, \Delta y, \Delta z$ are very small, equation 5-5 can be rewritten as follows

$$-\frac{\partial(\rho q_x)}{\partial x} - \frac{\partial(\rho q_y)}{\partial y} - \frac{\partial(\rho q_z)}{\partial z} \pm R = \frac{\partial(\alpha\rho)}{\partial t} \tag{Eq. 5-7}$$

Moreover, due to the low compressibility of water, ρ can be assumed constant. Therefore, $\frac{\partial(\alpha\rho)}{\partial t}$ shows the volume change of water-bearing cell which due to the constant dimensions of the cell, this volume change is expressed as change in the height. Having h as the height of water in the cell and Ss as the storage coefficient, we will have:

$$\frac{\partial(\alpha\rho)}{\partial t} = S_s \frac{\partial h}{\partial t} \tag{Eq. 5-8}$$

Using the mentioned equations, equation 5-7 can be rewritten as follows:

$$-\frac{\partial(q_x)}{\partial x} - \frac{\partial(\rho q_y)}{\partial y} - \frac{\partial(q_z)}{\partial z} \pm R = S_s \frac{\partial h}{\partial t} \tag{Eq. 5-9}$$

If the values of q_x, q_y and q_z obtained from equation 5-6 is replaced in equation 5-9, the 3-Dimensional groundwater flow in the instable condition in the porous media with constant specific weight is expressed by the differential equation of 5-10. Based on this equation, the algebraic sum of water flow in the 3 principal directions plus the recharge and discharge water is equal to the water volume change of the cell.

$$\frac{\partial}{\partial x}\left(k_x \frac{\partial h}{\partial x}\right) + \frac{\partial}{\partial y}\left(k_y \frac{\partial h}{\partial y}\right) + \frac{\partial}{\partial z}\left(k_z \frac{\partial h}{\partial z}\right) \pm R = S_s \frac{\partial h}{\partial t} \tag{Eq. 5-10}$$

Where:
h: Hydraulic head [L]
R: flow volume per unit volume which shows the increasing or decreasing source [F^{-1}]
Ss: storage coefficient of porous media [L^{-1}] and t: time [T]

The numerical method to solve groundwater flow equations in MODLOW is the finite difference method. In this method, the continuous system of equation 5-10 is substituted with some distinct points in space extent and the partial derivatives are written as equations based on hydraulic head difference in these points. Therefore, it will have the system of linear algebraic equations that is solve for the hydraulic head values in the designated points and in the designated time. The obtained solution is an acceptable approximation of hydraulic head.

5.2. MODFLOW

As described in Section 2, the MIPWA model is based on the MODFLOW groundwater flow model (McDonald and Harbaugh, 1988). MODFLOW is a simulating computer program using the finite difference method to model 3-Dimensions groundwater flow in porous media. The partial differential

equation (Eq. 5-10); (USGS, 2005); is used to express the 3-Dimensions groundwater flow in a porous media with constant density.

MODFLOW code is a finite-difference modular groundwater flow model. The modular structure of the computer program consists of main program and an array of completely independent sub-routines which are called "Modules". Modules are grouped in "Packages". Each package relates to a distinct hydrologic system which has to be simulated. The groundwater recharge module returns for each time step.

The groundwater flow in the aquifer is simulated by cell centred finite difference method. Layers can be simulated as confined, unconfined and a combination of confined and unconfined. Flows with external tensions such as wells, local recharge, evapotranspiration, drainages and rivers can also be simulated. MODFLOW program is written in FORTRAN77 language. In short, after writing the finite difference equation for all active groups in the grid, an equation system with "n" equations and "n" unknowns is obtained. In this method, the iteration method is implemented in such a way that the whole algebraic equation system contains an equation for each calculation cell in the grid. In this form, the equations system can be rewritten and solved as a matrix.

Spatial division of the aquifer is possible by a network of 3D-blocks which are called cells in the model approach. The location of each of the blocks is based on spatial indices by rows, columns and layers indictors as designated by i, j and k indices respectively. (Figure 5-1)

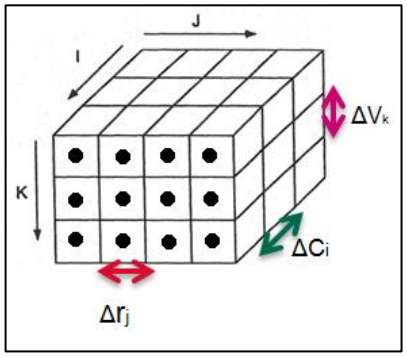

Figure 5-2 Grid structure of the model domain area

At the centre of each cell a (calculation) node with specific indices is defined. These nodes are chosen such that the aquifer is gridded with parallel and perpendicular lines where the nodes are placed in the centre of the formed cells. The same is applied in vertical perspective so following this order hydraulic head values, Φ , are estimated for each calculation node, and thus each cell, for each model time step. The Darcy equation applies to each cell in the horizontal and vertical directions and it will be as follows for each direction: In the horizontal flow direction:

$$Q = kA\left(\frac{\emptyset 2 - \emptyset 1}{\Delta r}\right) \qquad \text{(Eq. 5-11)}$$

Where:
Q: amount of water flow [L^3/T]
Φ: hydraulic head [L]

A: horizontal flow cross section [L^2] which is equal to $\Delta C \times \Delta V$
K: hydraulic conductivity [L/T]
Δr: horizontal distance between two cell boundaries [L]

Since in the horizontal direction, the area of flow is equal to the thickness of the cell of layer (A=D), the amount of flow from the cross section is equal to:

$$Q = kD\left(\frac{\Delta \emptyset}{\Delta L}\right) \quad \text{(Eq. 5-12)}$$

In the vertical flow this reads:

$$Q = KA\left(\frac{\emptyset 2 - \emptyset 1}{\Delta V}\right) \quad \text{(Eq. 5-13)}$$

where:
Q: the amount of water flow [L^3/T]
A: vertical flow cross section [L^2] which is equal to $\Delta C \times \Delta r$
K: hydraulic conductivity [L/T]
ΔV The vertical distance between two cell centres [L]

In this condition, the distance between two hydraulic heads will be equal D, thus

$$Q = KA\left(\frac{\emptyset 2 - \emptyset 1}{D}\right) \text{ or } Q = \frac{K}{D}A(\emptyset 2 - \emptyset 1) \quad \text{(Eq. 5-14)}$$

in which:
$\frac{K}{D} = Le\ [T^{-1}]$ is the leakage coefficient which is the reciprocal of hydraulic resistance (C)
Therefore the Darcy equation will be as:

$$Q = \frac{1}{C}A(\Delta \emptyset) \quad \text{(Eq. 5-16)}$$

6. RESULTS AND DISCUSSION

6.1. Analysis of SEBAL based ETa maps

By the research objectives of this study, results of ETa estimates by the MIPWA-CAPSIM model are compared to the satellite based SEBAL estimates. For this purpose the satellite images require validation to evaluate if images can serve as a reference and possible calibration target to the model simulated ETa. If images prove to be unreliable there is no reference for comparison to calibrate the model.

For this study, by the constraint of the MIWPA-CAPSIM model to only generate ETa output at yearly base, the satellite images at daily base are accumulated to yield equivalent estimates. For these cumulative maps for 8 months are created for which SEBAL estimates were available. These maps serve to assess seasonal distribution of ETa across the study area but also to evaluate magnitude and representativeness of ETa estimates for the various seasons. Below, the images for the months of March and April refer to the year 2013, for the other months (i.e. May, June, July, August, September and October) images refer to the year 2012. By unavailable of images from November, December, January and February, these months are ignored in the comparison. It is noted that the period November – February largely overlap the winter season for which the ETa fluxes only are very small and only a fraction of the summer and spring ETa. Reference is made to Figure 6-6 where it is shown that ETa in the winter period has average value of 5 mm per month (1950-1970).

For comparison of seasonal ETa, maps of monthly evapotranspiration are prepared. For the spring, summer and autumn season, maps are summed and averaged to come up with mean estimates. For spring season maps for the month March (2013), April (2013) and May (2012) are used (Figure 6-1), for summer season June (2012), July (2012) and August (2012) are used (Figure 6-2) whereas for autumn season September (2012) and October (2012) are used (Figure 6-3). All maps are rescaled to the same value range. Simple visual inspection shows that maps have large resemblance with only little difference in seasonal ETa. Reference is made to Table 6-1 where minimum and maximum values of mean cumulative evapotranspiration for each season are shown. Monthly mean ETa over the study period is 59.1 mm.

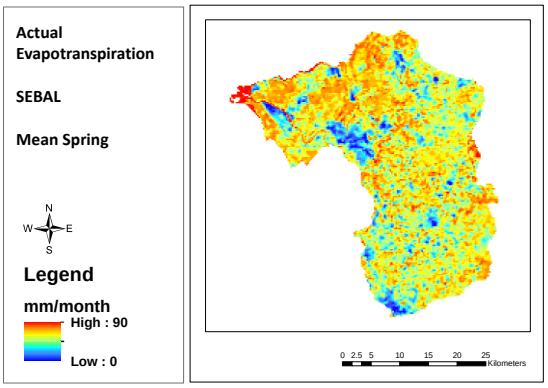

Figure 6-1, Mean SEBAL-based ETa for spring

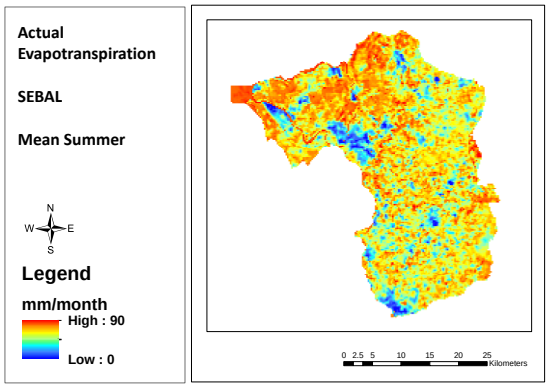

Figure 6-2, Mean SEBAL-based ETa for summer

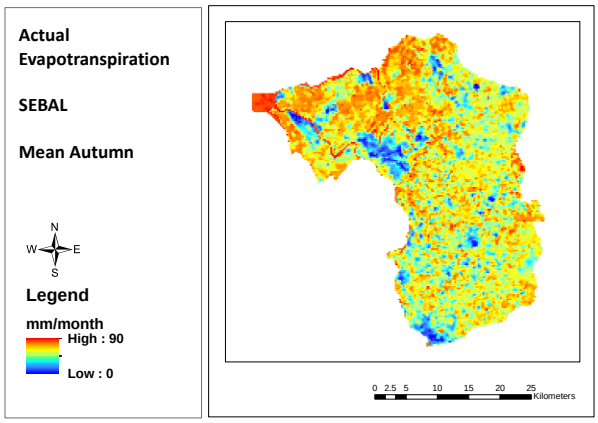

Figure 6-3, Mean SEBAL-based ETa for autumn

Table 6-1, Mean actual evapotranspiration for each season

	Mean Spring	Mean Summer	Mean Autumn
Minimum (mm)	22.8	24.7	22.4
Maximum (mm)	81.6	84.4	80.2
Mean (mm)	58.1	61.4	57.4
Standard deviation	9.8	9.9	9.7

To assess differences between the seasons and to assess any aspect of spatial variability, difference maps are prepared where the map of the summer season served as reference. This since ETa estimates in summer is highest in the Netherlands (Figure 6-6). Figure 6-4 shows results when ETa estimates for the spring season are deducted from summer season; Figure 6-5 shows results when ETa estimates for the autumn season are deducted from the summer season. Comparison of the difference maps only indicates little difference with largest value of 10mm. Surprisingly, for some river channels, the difference is at its largest values (10mm) while for other open water bodies differences are 0mm. For the south-eastern and eastern part, differences between the difference maps (summer and spring and summer and autumn) are largest. Differences between both periods, however, are relatively small with largest difference of approximately 5mm. As such, intermediate results of the various comparisons suggest that images are not very reliable. Further analysis aim at statistics of the image estimates with reference to Table 6.1.

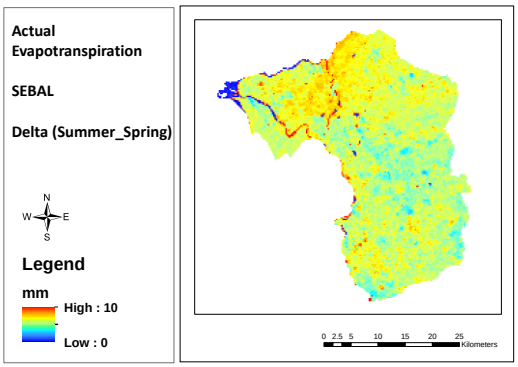

Figure 6-4 , Difference map of ETa between summer and spring seasons

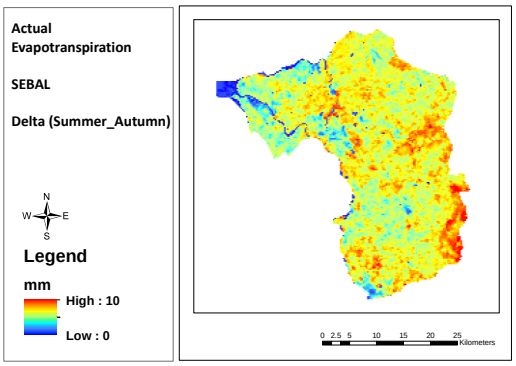

Figure 6-5 , Difference map of ETa between summer and autumn seasons

In Table 6-1 it is shown that mean monthly values for the respective seasons are very close to each other and suggest that ETa does not change much from spring to summer season and from summer to autumn season. Also standard deviations for respective seasons are of similar value and suggest that temporal variability is of similar behaviour. Both aspects of the small differences in average ETa as well as standard deviation also indicate that images are not very reliable since yearly and seasonal cycles do not match real world ETa cycles in the Netherlands. In this respect, it is noted that climatic factors affecting evapotranspiration such as temperature, sunshine hours, radiation and wind speed vary largely across the yearly cycle in the Netherlands. Reference is made to de Vries (1974) who showed that actual evaporation in Netherland is approximately 75% of the potential evaporation according to Penman (Figure 6-6), or 90% of the reference according to Makkink evaporation. Figure 6-6 shows monthly distribution values (1950-1970) of precipitation and potential evaporation according to Penman equation.

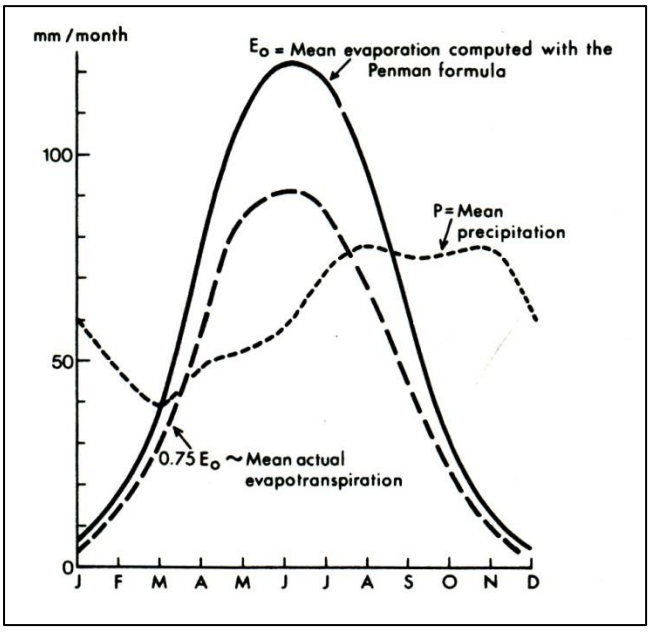

Figure 6-6, Relation between Penman evaporation and actual evapotranspiration (de Vries 1974) for (1950-1970).

ET_p in Salland study area is calculated based on Makkink method; and according to de Vries (1979), ET_a equals 90% of the ET_p calculated. Hiemstra and Sluiter (2011) in the KNMI technical report show ET_p values for CABAUW and WILHELMINADORP stations which are as shown in Table 6-2. Although stations do not reflect on large scale ETa estimates across the Netherlands and/or the Salland area, by lack of reliable station data in the study area, the estimates serve as a reference to the satellite based estimates. Based on de Vries (1979), the ET_a for these data sources are presented in the third column in Table 6-2 which shows estimates of $0.9 \times ET_p$. A histogram of ET_a and ETp is presented in Figure 6-7.

Table 6-2, Mean monthly Makkink evaporation (Hiemstra and Sluiter, 2011) and its ETa (de Vries, 1979)

Month	KNMI Makkink Evaporation	SD_KNMI Makkink Evaporation	KNMI ETa [Based on de Vries (1979)]
January	8.4	0.7	7.6
February	15.2	1.0	13.6
March	34.0	1.6	30.6
April	60.2	1.7	54.1
May	87.0	2.2	78.3
June	93.7	3.0	84.3
July	98.3	3.0	88.4
August	82.5	2.9	74.3
September	50.9	1.8	45.8
October	28.1	1.3	25.3
November	11.2	1.0	10.1
December	6.3	0.5	5.7

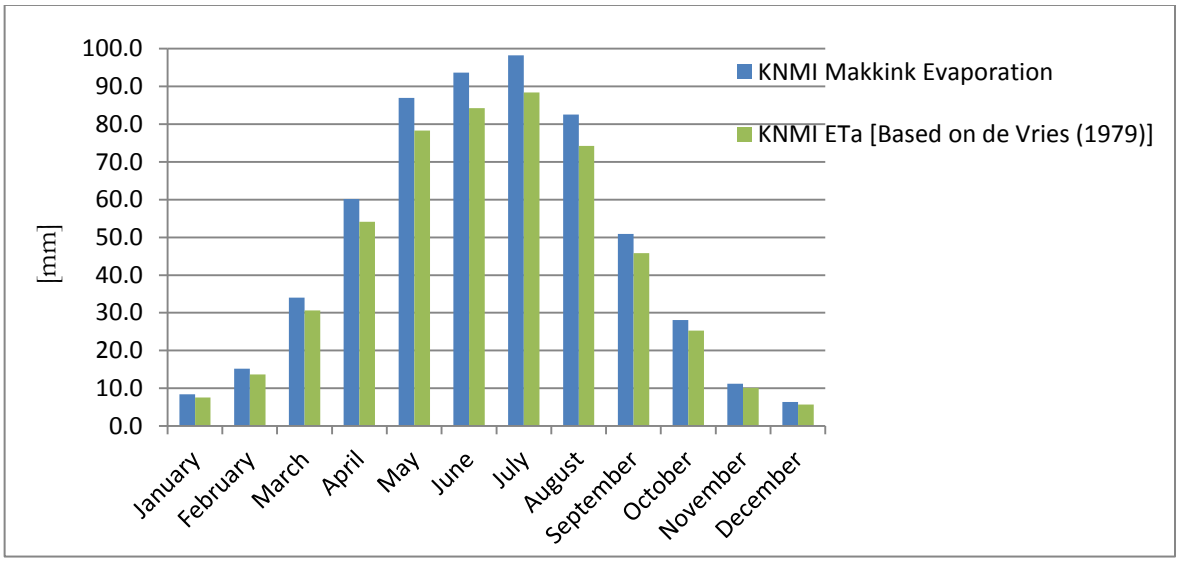

Figure 6-7, Relation between Penman evaporation and actual evapotranspiration (de Vries 1974) for (1950-1970).

The SEABAL-based ET_a values for 8 months in the Salland area are also presented in Table 6-3. The total average for these 8 months is 59.1. The range of standard deviations in these 8 months shows that the variability of ET in these months is small which is contrary to the patterns for the two stations in the Netherlands.

Table 6-3, The SEABAL-based average ET_a values for 8 months

	March_13	April_13	May_12	June_12	July_12	Aug_12	Sept_12	Oct_12
Number of Pixels	50.616	50.616	51.330	51.330	51.330	51.330	51.330	51.330
Cumulative ETa (mm)	3.046.262	2.703.949	3.139.715	2.977.914	3.263.817	3.220.204	2.866.697	3.033.012
Minimum (mm)	23,4	19,4	23,4	22,7	25,5	24,9	21,8	23,1
Maximum (mm)	87,5	76,6	84,4	80,7	86,8	86,8	78,7	81,8
Mean (mm)	60,2	53,4	61,2	58,0	63,6	62,7	55,8	59,1
Standard Deviation	10,1	9,3	10,4	9,9	10,0	10,1	9,6	9,9

ETa estimates by de Vries (1974) and monthly normal variation of evapotranspiration in the KNMI technical report (Hiemstra and Sluiter, 2011) are quite different from the SEBAL-based estimates. A histogram on monthly estimates is shown in (Figure 6-8) and indicates large deviations. The SEBAL-based evapotranspiration tends to highly underestimate the KNMI based estimates for the summer period but largely overestimates the spring and autumn period, in particular. Overall and in conclusion, it seems that the SEBAL-based images are not suitable to serve as reference for the MIPWA-CAPSIM estimated actual evapotranspiration in the study area.

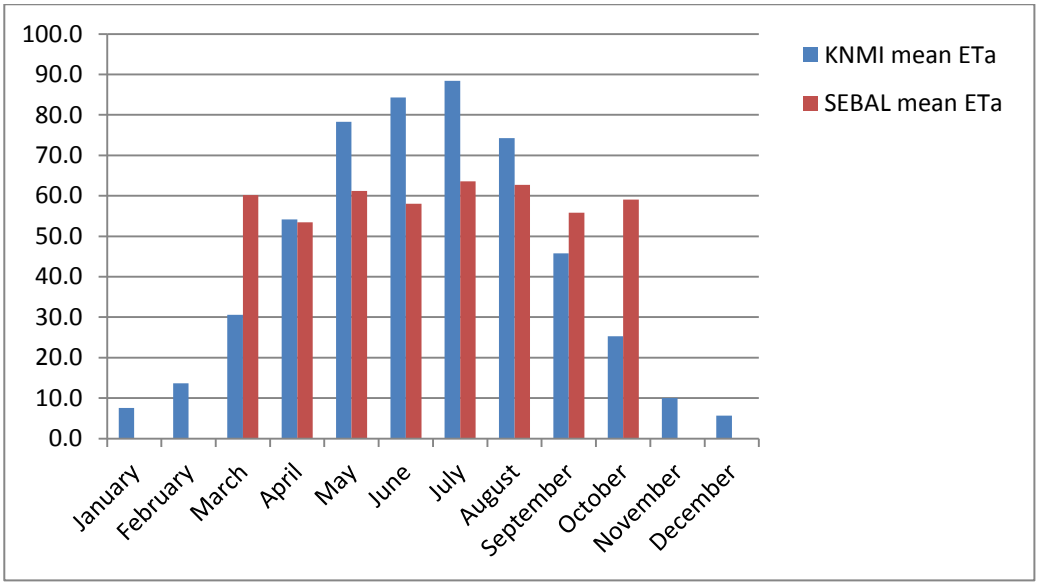

Figure 6-8, comparing KNMI ETa and SEBAL-based ETa

6.2. Analysis of MIPWA-CAPSIM based ETa map

MIPWA-CAPSIM provides a map of the cumulative ET_a for the period 1-5-2012 to 1-5-2013 (Figure 6-9) that covers a 12-month period including all 4 seasons. By evaluating the one-year cumulative ET_a map by the model, the accuracy of MIPWA is investigated. Figure 6-10 also shows cumulative SEBAL-based map for the 8 month period.

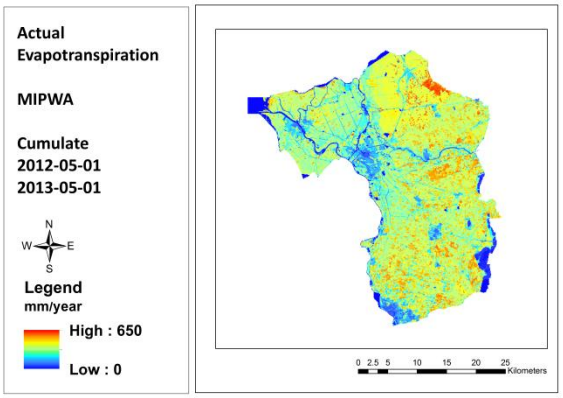

Figure 6-9, Cumulative ETa map for 2012-2013 provided by MIPWA-CAPSIM

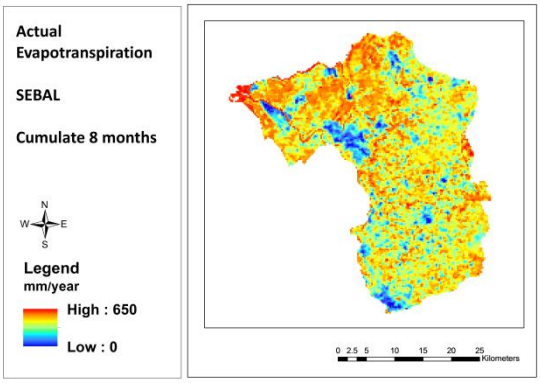

Figure 6-10, SEBAL-based cumulative ETa map for 8 months

Although temporal scale of SEBAL-based cumulative ETa (Figure 6-10) is smaller than MIPWA-CAPSIM based cumulative ETa (Figure 6-9), based on Table 6-4 values it can be noted that SEBAL-based ET_a had large over-estimation compared to MIPWA-CAPSIM method, such that minimum ET_a based on MIPWA-CAPSIM is 0 mm, while in SEBAL method it is 207.7 mm. This over-estimation is also significant in spatial distribution. In other words, SEBAL method had over-estimation in most of the places, where the extent of areas with maximum or near-maximum ET_a in SEBAL method is much higher than MIPWA-CAPSIM method in north and northwest of the region.

As addressed before, computation of evapotranspiration in a difficult modelling task. Since figures 6-9 and 6-10 are model outputs of 2 different models and in the modelling process, conditions are to be simplified, the model results are different from real conditions in the nature. Although, as depicted in figure 6-8, in March, September and October, SEBAL model had over-estimations compared to the mean variation trends of ETa in the Netherlands which are shown in figure 6-10 as near-maximum values. Due to the lack of monthly mean values for MIPWA model output and the inability to compare them with variation trends in the Netherlands, it is not possible to judge on which method output is closer to the real values. Therefore, in-situ data should be collected from designated stations in the region to be able to judge on which of SEBAL-based or MIPWA-based maps are closer to the natural conditions.

Table 6-4, Statistic of cumulative ETa maps provided by MIPWA-CAPSIM and SEBAL-based

	MIPWA (one year)	SEBAL (8 months)
Minimum (mm)	0	207.7
Maximum (mm)	572.6	648.6
Mean (mm)	329.2	492.4
Standard Deviation	90.9	63.8

In figure 6-9 minimum amount was 0 mm for open water which is due to applying boundary conditions in the model. Since water level variations are so small compared to the water body, the model considered this amount to be zero. Moreover, in southeastern parts of the region, due to woody vegetation cover and dry areas, the ET is considered to be zero for the MIPWA-based model. Although, in figure 6-10, the minimum value for the region is 207.7, for the purpose of comparing SEBAL-based and MIPWA-based maps, the minimum value was considered to be zero.

6.3. Feddes equation parameters in the Model

Based on (Eq. 4-1), to optimize the equation parameters, it is necessary to consider the ETa (or Ta) values and root zone for the plants and reduction coefficient for root water uptake. Also based on (Eq. 4-6), if the soil is unable to provide the plant with its water demands for maximum transpiration, reduction coefficient is deducted from maximum transpiration value.

In addition, based on the equations mentioned in section 4-3 regarding Feddes equation, higher maximum actual evapotranspiration results in smaller suitable areas for water absorption. In other words, the absolute value of pressure head or root zone thickness will be smaller. In contrast, lower ETa results in suitable conditions for more water absorption as well as larger absolute value of pressure head and root zone thickness.

Although, based on section 6.1 results, due to the lack of reliability of SEBAL-based ETa maps, its values were not compared with MIPWA method ETa. However, it seems that, in case a significant relation is found between the values in these SEBAL and MIPWA-CAPSIM methods, this relation may be added as a coefficient to Zr values in ROOT_SIM and UNSA_SIM files in the CAPSIM part (see section 4-1). For more investigations, more detailed studies are required in the future.

6.4. Analysis of Classified MIPWA-CAPSIM based cumulative ETa map

As depicted in the cumulative map (Figure 6-11), Salland area can be categorized into 4 classes based on the ET_a depth which are: very low ETa , low ETa, medium ETa and high ETa.

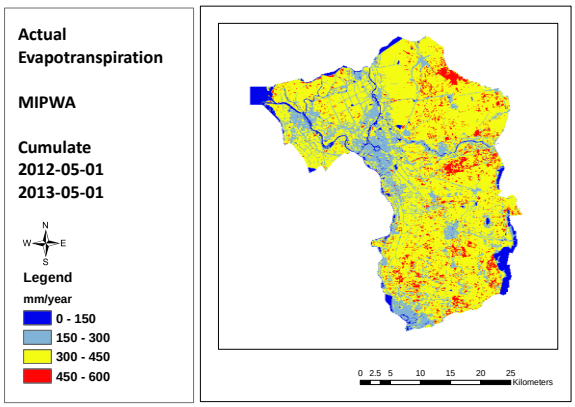

Figure 6-11, Classified cumulative ETa map provided by MIPWA for one year

Very low ETa (0-150mm): based on Figure 6-11 the south-eastern part of the Salland area is a heathland with very low ET_a. The heathlands are generally woody vegetation in dry area. Estimates

for canals, streams and open waters in general show very low ET_a but is the result of the imposed boundary condition where ETa is set to zero.

Low ETa (150-300mm): includes the Zwolle, Deventer and Kampen urban areas which have low ET due to the asphalt cover and lack of vegetation on the soil surface.

Medium ETa (300-450mm): constitutes a large percentage of the Salland area and indicates farms and pasturelands which have medium high ET_a values due to the presence of sufficient moisture and vegetation.

High ETa (450-600mm): includes the mixed forest areas in the central eastern part of Salland in the south of Vecht River and Landgoed Visteren as well as mixed forests including broadleaf trees and pasturelands in the northeast of the area which have high ET due to the high concentration of vegetation.

There are few important system-characteristic that affect ET_a :

1. Land use: ETa is directly dependent on the landuse. ETa is higher in the areas with more soil cover and it increases by the presence of vegetation. Large and deep rooted vegetation easily abstracts soil water by their roots and causes more transpiration. Figure 6-12 shows example areas 5, 6 in the Salland area and shows farmlands 4. In contrast, in the areas 1, 2 and 3, by to the smaller soil surface, less ETa will occur.

2. Elevation: Based on the digital elevation map of the area (Figure 3-3), elevation of Salland area decreases from southeast with 60 m and more to northwest with -2 m or less. As depicted in Figure 6-9, in the southeast of the heathland it seems that the type of vegetation and lack of root access to the water in the unsaturated zone, resulted in the decrease of plants transpiration and thus ET_a. However, since the ET_a has larger values in central and northeast of the area, the effect of elevations seems to be less significant.

Since the MIPWA-CAPSIM model produces the cumulative map for a one year period, areas with constant land cover have high ET_a values. This applies, e.g. to forested areas, since the land cover does not change during the modelling period. Due to large cumulative evaporation from the soil and transpiration from the trees, ET_a has high value. In farmlands, however, due to the cultivation period which is shorter than one year, the cumulative ET_a will be lower. If the evaluation is done on a daily basis, the ET_a of a farmland in the cultivation season might be higher than forest areas.

The important point is the low amounts of ET_a in open water in the northwest of the area and the surface of the canals, in which, is caused by the imposed boundary condition (constant head).

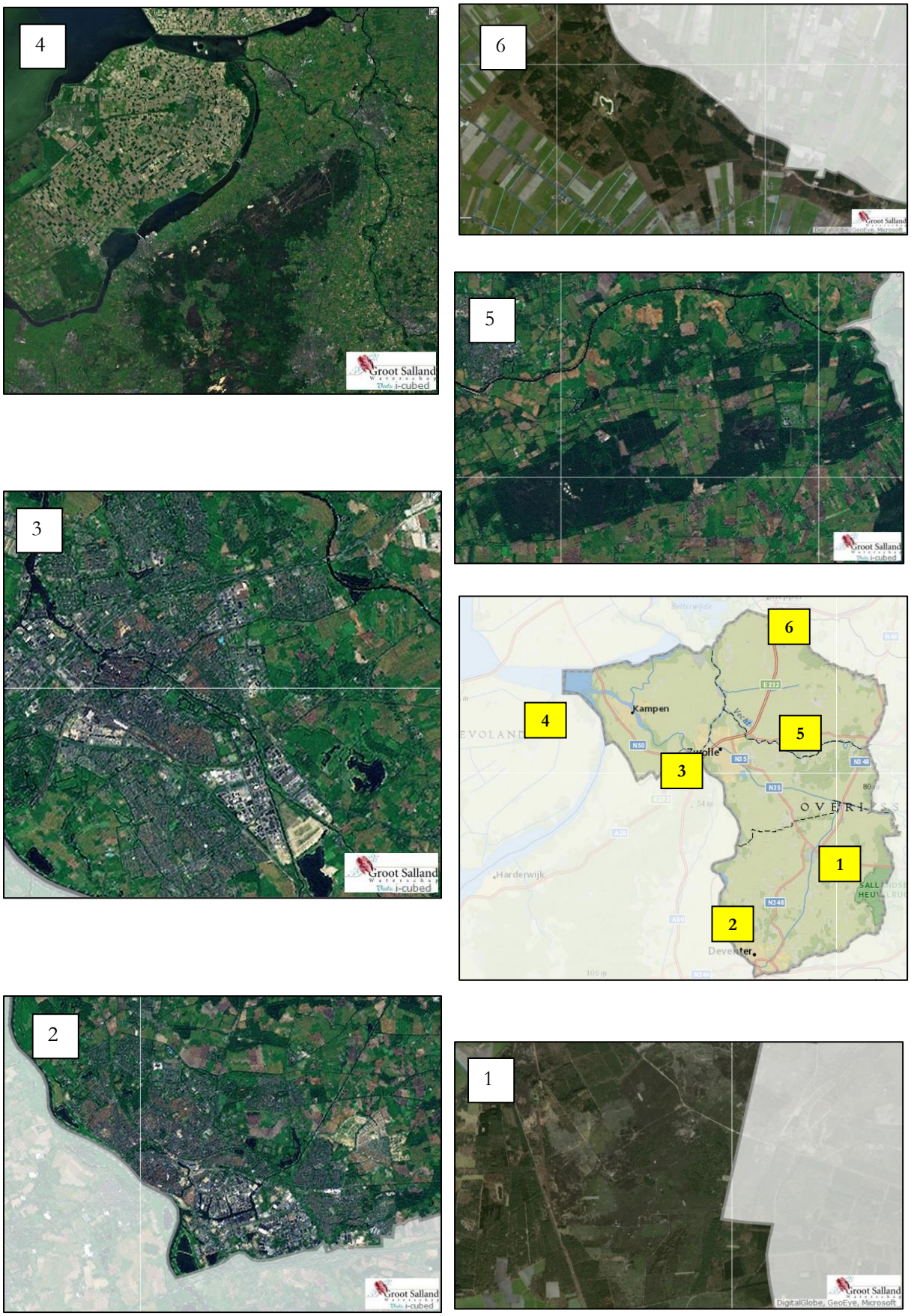

Figure 6-12, Satellite images of land use in Salland area

6.5. Hydraulic head and groundwater level

To evaluate the groundwater level, seasonal mean hydraulic heads estimates of different layers were converted and represented in a map for each layer. Since ETa mostly affects recharge and the groundwater level in the first layer, only these result are discussed. The remaining maps for mean seasonal hydraulic head of layers 2, 3, 4, 5, 6 and 7 are presented in the Appendix 3. The model output for each month was in 14th and 28th. Figures 6-13 shows mean seasonal hydraulic head for March (2013), April (2013) and May (2012) for spring. Figure 6-14 shows mean value of June (2012), July (2012) and August (2012) for summer season. Figure 6-15 for shows mean of September (2012), October (2012) and November (2012) for autumn and Figure 6-16 shows mean hydraulic head for December (2012), January (2013) and February (2013) for winter season. In spite of different precipitation and ET amounts in different seasons, the highest hydraulic head was observed in the southeast area of the region which based on figure 3-3 has the highest elevation. The mean hydraulic head in different seasons were similar for some parts but differed well for other parts suggesting temporal variation by recharge inputs and ETa losses.

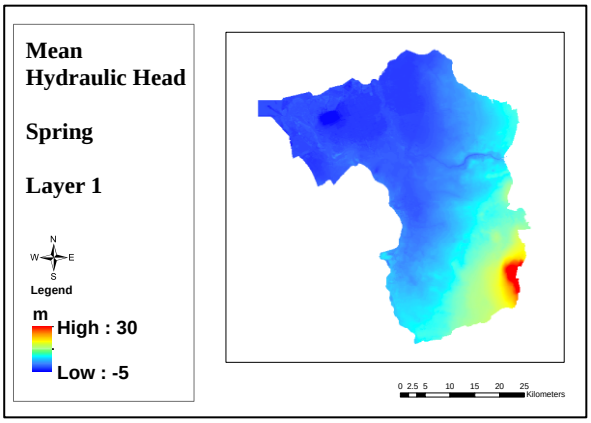

Figure 6-13, Mean hydraulic head of layer 1 for spring

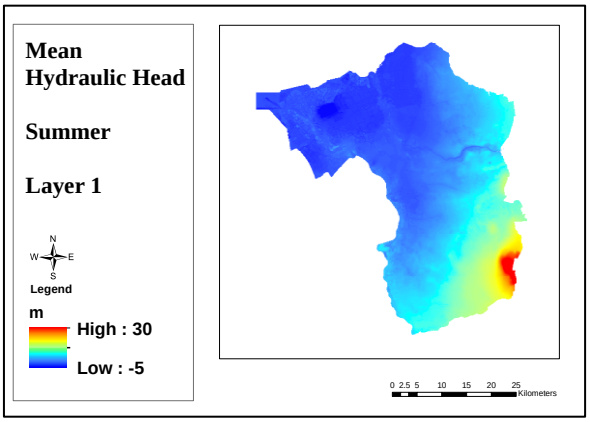

Figure 6-14, Mean hydraulic head of layer 1 for summer

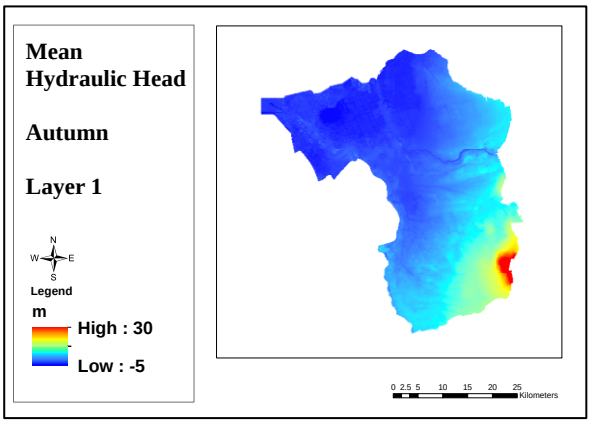

Figure 6-15, Mean hydraulic head of layer 1 for autumn

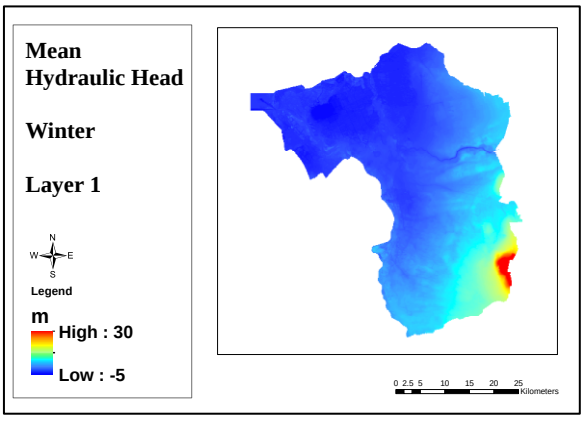

Figure 6-16, Mean hydraulic head of layer 1 for winter

Table 6-5 shows statistics of the maps. The range of variations in different seasons for lowest (minimum) values only is very small but for maximum (highest) values differences are as large as 7m. Standard deviation for all seasons is in the range 3,5 – 4,0 meter.

Table 6-5, Statistics of mean seasonal hydraulic head maps

	Mean Spring	Mean Summer	Mean Autumn	Mean Winter
Minimum [m]	-3.75	-3.75	-3.79	-3.79
Maximum [m]	22.07	21.40	25.98	29.85
Mean [m]	2.44	2.56	3.01	2.83
Standard deviation	3.49	3.47	3.91	4.06

Figures 6-17, 6-18, 6-19, 6-20 show mean seasonal groundwater level similar to the months which are selected for mean hydraulic head. Variation in groundwater levels were influenced by hydraulic head such that the lowest value was for the northwest of the region due to the low elevation, being near open-water level and being an area for accumulation of water on the ground.

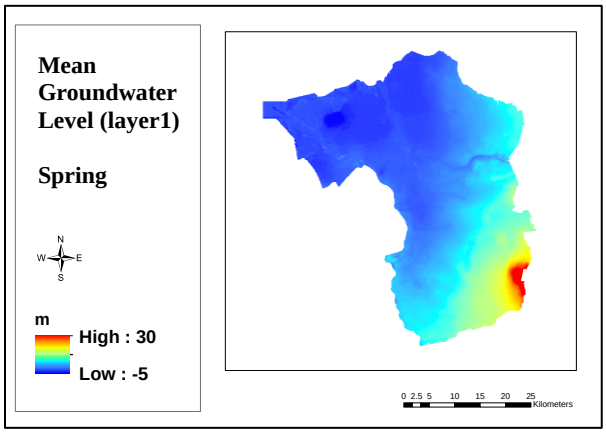

Figure 6-17, Mean groundwater level of layer 1 for spring

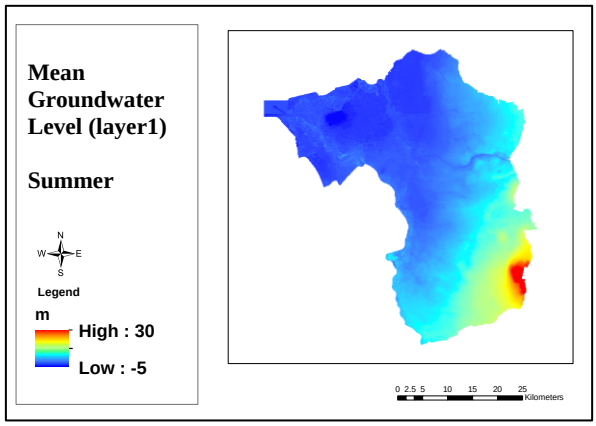

Figure 6-18, Mean groundwater level of layer 1 for summer

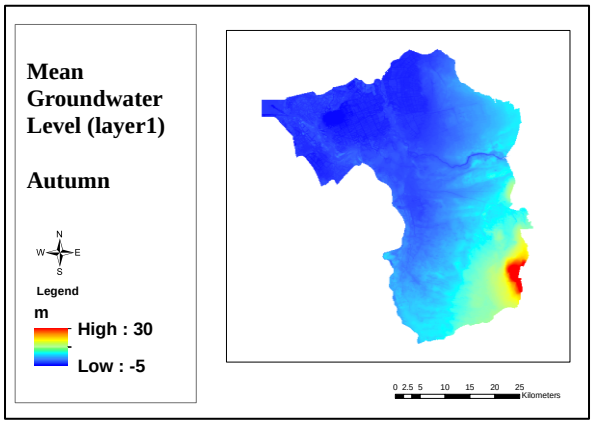

Figure 6-19, Mean groundwater level of layer 1 for autumn

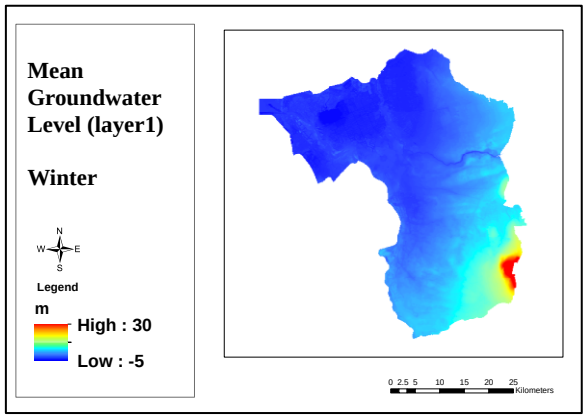

Figure 6-20, Mean groundwater level of layer 1 for winter

Table 6-6 shows statistics for mean seasonal maps. The highest value in winter might be because of high precipitation and low evapotranspiration. This table shows that despite the seasonal variation in precipitation, temperature and ET, the range of variations in groundwater level were close to each other.

Table 6-6, Statistics of mean seasonal groundwater level maps

	Mean Spring	Mean Summer	Mean Autumn	Mean Winter
Minimum [m]	-3.77	-3.75	-3.79	-3.79
Maximum [m]	21.44	21.40	25.98	29.85
Mean [m]	2.36	2.56	3.01	2.82
Standard deviation	3.44	3.47	3.90	4.06

6.6. CAPSIM waterbalance and recharge estimation

Recharge estimation is an important part as well as a problem in transient model. Based on model outputs, the most similar and appropriate (but not necessarily accurate) method is the use of CAPSIM model for recharge estimation. The CAPSIM output determines the flux between the saturated and unsaturated zones. However, this is not exactly what this study is considering for recharge, since CAPSIM flux also includes the amount of water flux from storage to groundwater when there is a rise in groundwater level. Although this amount is higher than the net flux from precipitation and ET, but for a long period of time, the mean of this flux can be a good indicator for the recharge estimation.

Figure 6-21 shows CAPSIM results of mean seasonal (spring) water balance estimates where Q_{in} is the total amount of precipitation and capillary rise which enters the CAPSIM part and Q_{ont} is the evapotranspiration and transpiration from the root which leaves the CAPSIM part. For summer, autumn and winter results are shown in Figure 6-22, Figure 6-23 and Figure 6-24 respectively. Result are simulated for the 14th and 28th of each month which are selected for hydraulic head simulation.

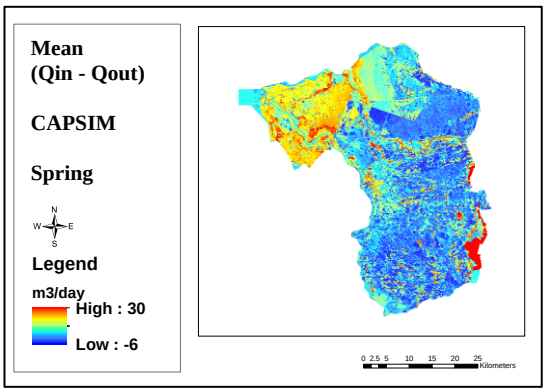

Figure 6-21, Mean water balance in CAPSIM for spring

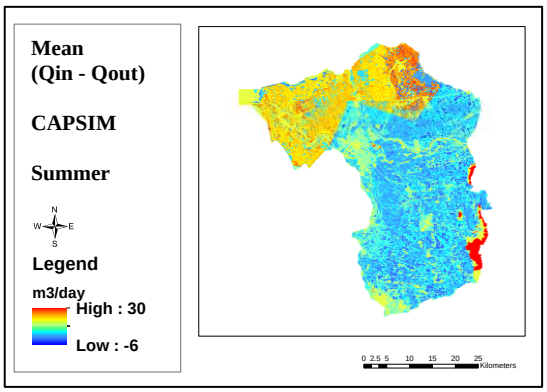

Figure 6-22, Mean water balance in CAPSIM for summer

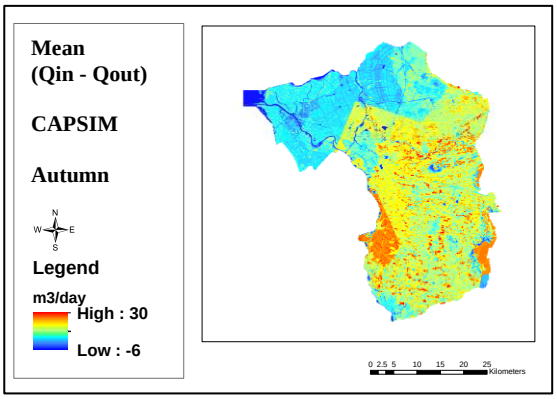

Figure 6-23, Mean water balance in CAPSIM for autumn

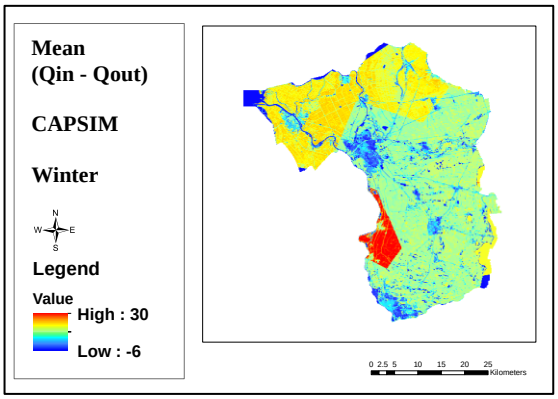

Figure 6-24, Mean water balance in CAPSIM for winter

Interpolation method was used to assign values to areas near the stations. Although this method is widely used in the hydrological studies, since these variations are not applied fuzzy, dividing the area to the Thyssen polygons is based on the location of data collection points. As a result, polygons shapes and their boundaries are not related to the distribution conditions of input and output values in the CAPSIM part. This is due to the fact that reading values from a station is used for the rest of the points in the polygon. This estimation has an error which cannot be quantified. Moreover, the neighbouring principle -which means that closer points are more similar compared to farther points- is not used in the polygons boundaries. In other words, variations are not fuzzy in the boundaries. The region have 12 stations and the abrupt variations in figures 6-21, 6-22, 6-23 and 6-24 are exactly on stations boundaries which is related to the collected data from each station.

Furthermore, Table 6-7 shows statistics for each map. Due to the lower precipitation in summer, maximum value for this season were lower than other seasons and autumn with the highest precipitation had the highest value.

Table 6-7, Statistics of mean seasonal water balance in CAPSIM part

	Mean Spring	Mean Summer	Mean Autumn	Mean Winter
Minimum [m^3/day]	-5,5	-5,0	-0,41	-2,5
Maximum [m^3/day]	18,6	6,3	28,0	23,2
Mean [m^3/day]	0,27	-1,4	9,1	7,2
Standard deviation	4,1	1,8	3,7	2,4

By using the mean seasonal variation shown for actual evapotranspiration (Figure 6-9) and groundwater levels (Figures 6-17, 6-18, 6-19 and 6-20), this could explain the amount of influx and outflux in CAPSIM as a unsaturated zone was obtained from the simulation results of MIPWA-CAPSIM model.

The high recharge values are estimated in areas that are mainly dominated by high elevated heathland areas (refer to Figure 6-12) while low values in low elevated areas covered by agricultural fields and urban areas. In contrast based on the cumulative ETa map (Figure 6-9) the calculated cumulative actual evapotranspiration for heathland in southeast of the region and agricultural fields and urban

areas is found to be lower than for mixed forest in northeast. This shows that loss of water from mixed forest contributes significantly to the total loss of water due to evapotranspiration.

The actual evapotranspiration from mixed forest is found to be higher than the other vegetation types in the area. The uniform land cover during the year and favourable conditions for transpiration from the vegetation and evaporation from soil surface contributes to the high ET in these areas and low recharge in these areas.

As a result, the high flux of inflow to the saturated zone from CAPSIM below the heathland is found to be higher than mixed forest and agricultural and urban areas. The lowest flux was obtained below agricultural and urban areas in a large portion of the area. However in autumn and winter, the southwest of the area has surprisingly high values.

Table 6-7 also shows that in autumn and winter seasons the highest estimated recharge fluxes are from the area covered by heathland. This shows that these vegetation types have a dominant effect on the groundwater recharge of the study area. The seasonal water balance in CAPSIM is found the estimated recharge flux shows a high temporal variability and follows a pattern similar to steady state result by model. (Figure 6-26)

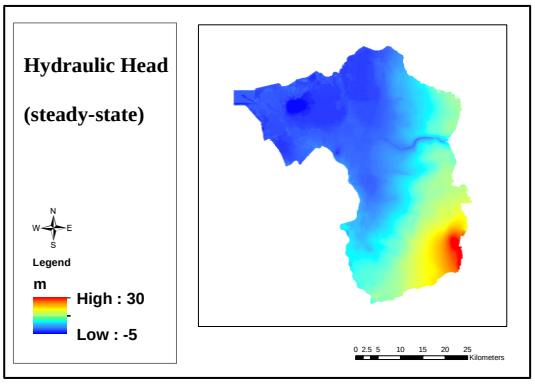

Figure 6-25, Hydraulic head for steady-state model

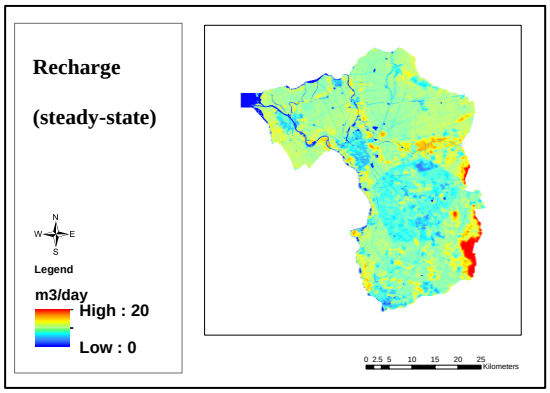

Figure 6-26, Recharge estimated value for steady-state model

Table 6-8, Statistics of hydraulic head map (steady-state)

	Hydraulic Head [m] (steady-state)
Minimum	-3,7
Maximum	15,6
Mean	2,2
Standard deviation	3,2

Table 6-9, Statistics of recharge map (steady-state)

	Hydraulic Head [m] (steady-state)
Minimum	-3,7
Maximum	15,6
Mean	2,2
Standard deviation	3,2

7. CONCLUSIONS AND RECOMMENDATIONS

7.1. Conclusions

The objective of this study was to evaluate how in groundwater modelling recharge was affected when satellite-based evapotranspiration was used instead of in-situ based ET in the Salland area.

Simulation results for this study are estimates of i) cumulative SEBAL-based and MIPWA-CAPSIM based ET_a, ii) mean seasonal hydraulic heads for each of the 7 layers, iii) groundwater level fluctuations and iv)) mean seasonal water balance for CAPSIM for the period 01-05-2012 to 01-05-2013.

Cumulative monthly and seasonal SEBAL-based ET_a maps were produced. Comparison with ET_a for the Netherlands showed than SEBAL-based maps were not reliable. Map could not serve for comparison of MIPWA-CAPSIM simulated ETa. Therefore, optimizing root zone parameters was not possible in the CAPSIM model and thus requires more detailed study in the future.

Cumulative ET_a was produced as classified maps by the model. Highest ET_a (579 mm) was in the northeast with mixed forests (Boswacterij Staphorst). The central east of the region in the southern part of Vechet River with mixed forests (Landgoed Vilsteren) has ETa of 498 mm and in diffuse areas in the southern part of the region. The lowest ET_a was in the southeast of the region (Hellendoornsche Berg) with heath woody vegetation (≈ 0 mm), that possibly is unrealistic. In areas with high ET_a due to the permanent vegetation cover and sufficient soil surface, the conditions were more favourable. In areas with low ET_a due to the wood vegetation cover and dry conditions and in urban areas due to the lack of soil surface and vegetation cover, the conditions were not favourable.

Variations in hydraulic head in the region were evaluated as seasonal mean values for each layer which showed that these variations are mainly following a particular trend. The range of variations in hydraulic head in different seasons for lowest (minimum) values only is very small but for maximum (highest) values differences are as large as 7m. Standard deviation for all seasons is in the range 3,5 – 4,0 meter.

Variation in groundwater levels were influenced by hydraulic head such that the lowest value was for the northwest of the region due to the low elevation, being near open-water level and being an area for accumulation of water on the ground.

Groundwater level variations in the first layer was also investigated in the form of seasonal mean which showed that the hydraulic gradient was from southeast (maximum value) to northwest (minimum value) of the region which depicts the groundwater flow direction.

The mean seasonal water balance in CAPSIM was evaluated to represent recharge estimation in the first layer. The highest flux was for autumn season equal to 28 m^3/day as recharge and the lowest flux was -5.6 m^3/day in spring as discharge. The spatial distribution also shows that maximum recharge estimation was in the southeast of the region due to the lack of vegetation cover and high groundwater level. Also, the minimum groundwater recharge was obtained below urban and agricultural areas in a northwest of area.

7.2. Recommendations

- Using MIPWA model with fixed geo-hydrological parameters such as c-value and KD-value for large areas in the region may cause some errors. It might be better to use this model for small study areas with optimized parameters which are closer to the natural conditions.

- Since the ET potential in this study was based on the data available from 2 stations close to the area and the data from 12 meteorological stations in the area were not available, including data from these stations may increase the accuracy of results in the future studies.

- Access to reliable satellite maps is required to optimize root zone parameters in Feddes equation for future studies.

- Developing the model program to produce daily ETa maps instead of annual cumulative ones will increase the accuracy of assessments.

LIST OF REFERENCES

- Bastiaanssen WGM, Menenti M, Feddes RA and Holtslag AAM, (1998): *Remote sensing surface energy balance algorithm for land (SEBAL)*: 1. Formulation. J. Hydrol., 212-213(1-4), 198-212
- Bastiaanssen, W. G. M., Menenti, M., Feddes, R.A., Holtslag, A.A.M. (1998a). *"A remote sensing surface energy budget algorithm for land (SEBAL). 1. Formulation.*" Journal of Hydrology 212 - 213(1-4): 213.
- Bastiaanssen, W. G. M., Pelgrum, H., Wang, J., Ma, Y., Moreno, J.,Roerink, G. J., and van der Wal, T. (1998b). *"The surface energy balance algorithm for land (SEBAL), Part 2: Validation."* J. Hydrol., 212-213, 213–22
- Bauer P, Gumbricht T and Kinzelbach W. (2006). *A regional coupled surface water/ground water model of the Okavango Delta, Botswana*. Water Resources Research, 42, W04403, doi: 10.1029/2005WR004234Vol.
- Berendrecht, W. L., Snepvangers, J. J. J. C., Minnema, B., & Vermeulen, P. T. M. (2007, December). *MIPWA: A Methodology for Interactive Planning for Water Management. In MODSIM 2007 International Congress on Modelling and Simulation.* Modelling and Simulation Society of Australia and New Zealand (pp. 74-80).
- Ben-Dor, E., Kindel, B. & Goetz, A.F.H. (2004). *Quality assessment of several methods to recover surface reflectance using synthetic imaging spectroscopy data.* Remote Sensing of Environment, 90, 389-404.
- Becker, M.W. (2005). *Potential for Satellite Remote Sensing of Ground Water.* Groundwater Vol. 44(2), pp. 306–18.
- Bouwer, H. 1978. *Groundwater Hydrology.* New York: McGraw-Hill Book Company.
- Brunner, P., Hendricks Franssen, H.J., Kgotlhang, L., Bauer-Gottwein, P., Kinzelbach, W. (2007). *How can remote sensing contribute in groundwater modelling?* Hydrogeology Journal Vol. 15(1), pp. 5–18.
- Brunner, P., Bauer, P., Eugster, M. and Kinzelbach, W. (2004). *Using remote sensing to regionalize local precipitation recharge rates from the chloride methods.* Journal of Hydrology, Vol. 294(4), pp. 241–50.
- Chabrillat, S., Goetz, A.F.H., Krosley, L. & Olsen, H.W. (2002). *Use of hyperspectral images in the identification and mapping of expansive clay soils and the role of spatial resolution*. Remote Sensing of Environment, 82, 431-445.
- De Vries, J.J., 1974. *Groundwater flow systems and stream nets in The Netherlands.* Ph.D. thesis, Vrije Universiteit, Amsterdam. Editions Rodopi, Amsterdam, 226 pp.
- De Vries, J. and Simmers, I. (2002). *Groundwater recharge: an overview of processes and challenges. Journal of Hydrogeology.* 10:5–17. DOI 10.1007/s10040-001-0171-7
- Feddes, R.A., Kowalik, P.J. and Zaradny, H., 1978. *Simulation of field water use and crop yield.* PUDOC, Wageningen, Simulation Monographs, 189 pp.
- Feddes, R.A., Raats, P.A.C., (2004). *Parameterizing the soil-waterplant root system. In: Feddes, R.A., et al. (Eds.), Unsaturated-zone modelling: Progress, challenges and applications.* Wageningen UR Frontis Series. Kluwer Academic Publishers, Dordrecht, The Netherlands, pp. 95– 141.

- Gao, Y., Long, D., Li, Z. (2008), *Estimation of daily evapotranspiration from remotely sensed data under complex terrain over the upper Chao river basin in north China.* International Journal of Remote Sensing, v.29, n. 11, p.3295-3315.
- Hendricks-Franssen, H.J.W.M., Brunner, P., Kgothlang, L. and Kinzelbach, W. (2006). *Inclusion of remote sensing information to improve groundwater flow modelling in the Chobe region.* IAHS, ModelCARE (Redbook series).
- Kampf, S. K., Tyler, S.W. (2006). *"Spatial characterisation of land surface energy fluxes and uncertainty estimation at the Salar de Atacama, Northern Chile."* Advances in Water Resources 29: 336- 354.
- Khalaf, A. and Donoghue, D. (2011). *Estimating Recharge Distribution Using Remote Sensing: A Case Study from the West Bank.* Journal of Hydrology (volume 414-415, p. 354-363).
- Kleidon, A & Heimann, M. (1998a) *Assessing the role of deep rooted vegetation in the climate system with model simulations: mechanism, comparison to observations and implications for Amazonian deforestation.* Clim. Dyn. in press .
- Kleidon, A & Heimann, M. (1998b) *A method of determining rooting depth from a terrestrial biosphere model and its impacts on the global water- and carbon cycle.* Global Change Biol. 4, 275-286.
- Kleidon, A & Heimann, M. (1998c) *Optimised rooting depth and its impacts on the simulated climate of an Atmospheric General Circulation Model.* Geophys. Res. Letts. 25, 345-348.
- Kumar, C.p. 1977. *Estimation of natural ground water recharge.* ISH Journal of Hydraulic Engineering 3(1): 61-74.
- Kumar, C.P. & Seethapathi, P.V. 2002. *Assessment of natural ground water recharge in upper Ganga canal command area.* Journal of Applied Hydrology 15(4): 13-20.
- Lerner, D. N.; Issar, A. S.; Simmers, I. (1990). *Groundwater recharge. A guide to understanding and estimating natural recharge.* IAH Int Contrib Hydrogeol 8. Heinz Heise, Hannover, 345 pp In: De Vries, J. and Simmers, I. 2002
- Lillesand, T.M., Kiefer, R.W. and Chapman, J.W. (2004). *Remote Sensing and Image Interpretation 5th edn.* John Wiley & Sons.
- Lubczynski, M.W. and Gurwin, J. (2005). *Integration of various data sources for transient groundwater modelling with spatio-temporally variable fluxes—Sardon study case, Spain.* Journal of Hydrology, Vol. 306(1–4), pp. 1–26.
- Makkink, G.F., (1957). *Testing the Penman formula by means of lysimeters. International.* Journal of Water Engineering, 11: 277-288
- Makkink, G.F., 1957. *Testing the Penman formula by means of lysimeters.* International Journal of Water Engineering, 11: 277-288
- Feddes, R.A., (1987). *Crop factors in relation to Makkink reference-crop evapotranspiration.* In: J.C. Hooghart (Ed.), Evaporation and weather. Proceedings and Information No. 39, TNO Committee on Hydrological Research, The Hague, pp 33-45.
- McDonald, MG and Harbough, AW. (1988). *A modular three-dimensional finite difference groundwater flow model.* US Geol Surv Tech Water Resour Invest., Book 6(Chapter A1).
- Molz, F. J. , and I. Remson, (1970). *Extraction term models of soil moisture use by transpiring plants.* Water Resour. Res, 6:1346-1356.
- Molz, F. J. , (1971). *Interaction of water uptake and root distribution.* Agron. J, 63, 608–610.

- Prasad, R. , (1988). *A linear root water uptake model.* J. Hydrol , 99:297-306. , P.A.C., 2004
- Santos, C., Bezerra, B., Silva, B., and Neale, C. (2009), *Assessment for daily actual evapotranspiration estimated by remote sensing algorithms.* Anais XIV Simposio Brasileiro de Sensoriamento Remoto, Natal, Brasil, 25-30 abril 2009, INPE, p. 427-434.
- Scanlon, B.R., Healy, R.W., Cook, P.G. (2002). *Choosing appropriate techniques for quantifying groundwater recharge.* Journal of Hydrogeology 10, 18–39
- Schmugge, T.J., Kustas, W.P., Ritchie, J.C., Jackson, T.J., Rango, A. (2002). *Remote sensing in hydrology.* Advances in Water Resources, 25, pp. 1367–85.
- Shaban, A., Khawlie, M. and Abdalla, C. (2006). *Use of GIS and remote sensing to detrnime recharge potential zones; the case of occidental Linanon.* Hydrogeology Journal, Vol. 14 (4), pp. 433–43.
- Shukla, S. & Jaber, F.H. 2006. *Groundwater recharge from agricultural areas in the Flatwoods Region of South Florida.* Edited by Department of Agricultural and Biological Engineering. 7: University of Florida.
- Sumioka, S.S. & Bauer, H.H. 2003. *Estimating ground-water recharge from precipitation on Whidbey and Camano Islands, Island County, Washington, water years 1998 and 1999.* In Water-Resources Investigations Report, 03-4101: Tacoma, WA: U.S.Geological Survey.
- Veldhuizen, A., P. van Walsum, A. Lourens and P. Dik (2006) *Flexible integrated modelling of groundwater, soil water and surface water,* in Poeter, E., C. Zheng, M. Hill, and S. Seo, Proceedings of MODFLOW and MORE 2006: Managing Groundwater Systems, IGWMC, Golden, Colorado, p. 94.
- Vermeulen, P.T.M., G. Hendriksen, J.J.J.C. Snepvangers, W.L. Berendrecht, A. Lourens, T. Tambach, T. Benedictus and B. Minnema (2006), *iMOD Interactive Modelling Environment. TNO Software,* www.tno.nl.
- Xi, C., Zhang, Z., Zhang, X., Chen, Y., Qian, M. & Peng, S. 2008. *Estimation of groundwater recharge from precipitation and evapotranspiration by Lysimeter measurement and soil moisture model.* Journal of Hydrologic Engineering 13(50): 333-340.

APPENDICES

APPENDICES 1, Descriptions of input files in iMOD

File	Description
PRF	iMOD Preference File
IMF	iMOD Meta File
IDF	iMOD Data File
IPF	iMOD Point File
IFF	iMOD Flow File
ISG	iMOD Segment File
GEN	ESRI Generate File
DAT	ESRI Generate File
ASC	ERSI Raster File
LEG	iMOD Legend File
CLR	iMOD Colour File
DLF	File containing color information to display boreholes
CRD	iMOD Coordinate File

APPENDICES 2, Descriptions of output results by runfile in iMOD

File (*.idf)	Variable	Description
bdgcap	Unsaturated Zone	Flux in/out CAPSIM
bdgbnd	Boundary Conditions	Flux in/out constant head boundaries
bdgfff	Flux Front Face	Flux in/out front cell faces
bdgflf	Flux Lower Face	Flux in/out bottom cell face
bdgfrf	Flux Right Face	Flux in/out right cell faces
bdgolf	Overland Flow	Flux out overland flow
bdgsto	Storage	Flux in/out storage
bdgwel	Wells	Flux in/out well systems
bdgdrn	Drainage	Flux out drainage systems
bdgriv	Rivers	Flux in/out river systems
head	Ground Water Head	Groundwater head
gwl	Groundwater level	Groundwater level
pwthead	Purge-water table	Purge-water table

APPENDICES 3, Mean seasonal hydraulic head for different layers

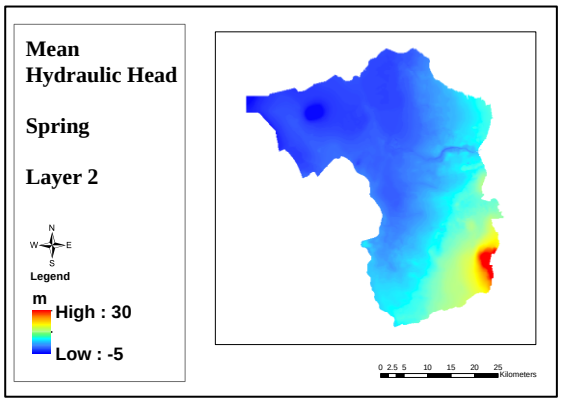

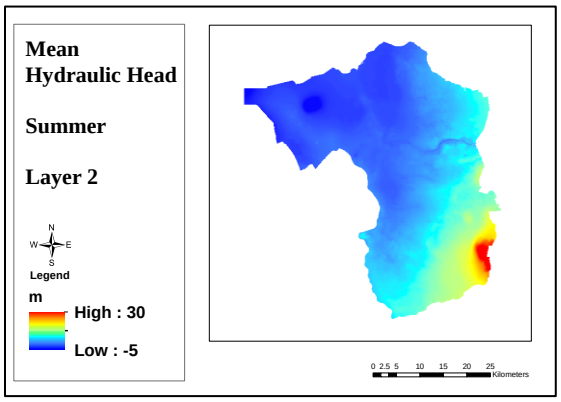

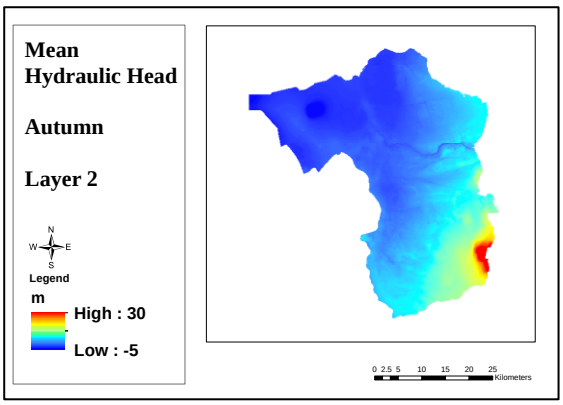

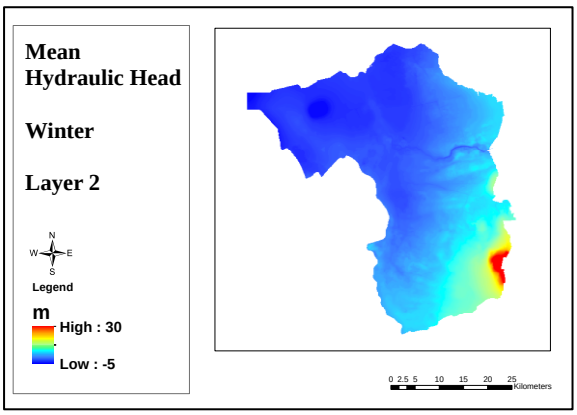

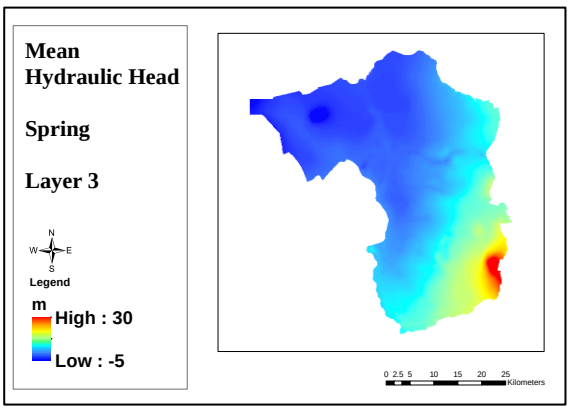

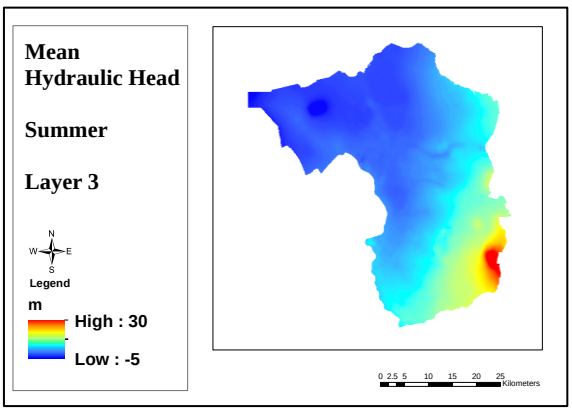

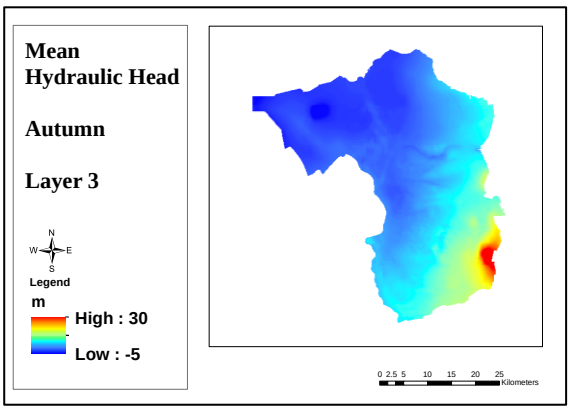

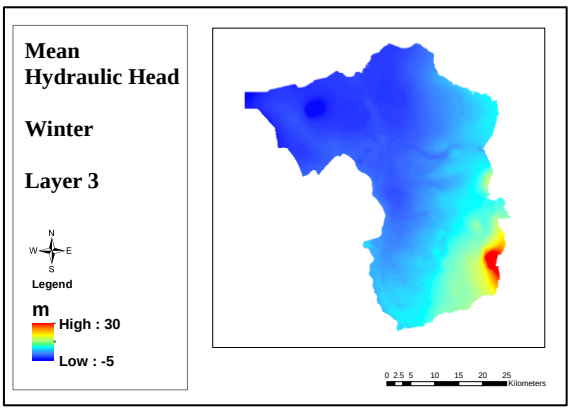

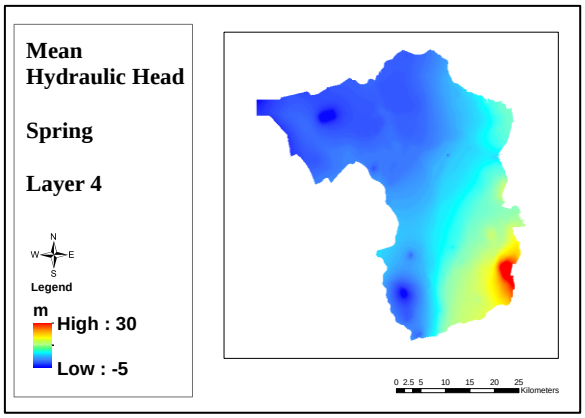
Mean
Hydraulic Head
Spring
Layer 4
Legend
m
High : 30
Low : -5
0 2.5 5 10 15 20 25
Kilometers

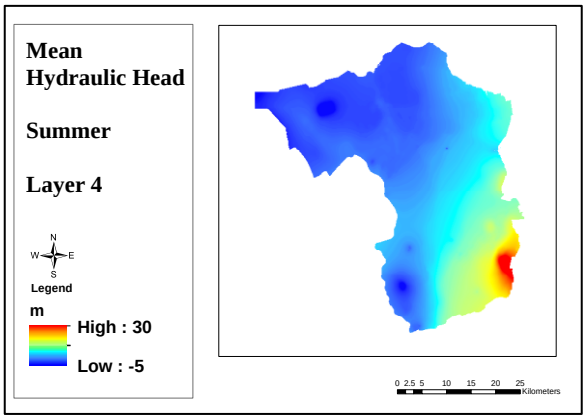
Mean
Hydraulic Head
Summer
Layer 4
Legend
m
High : 30
Low : -5
0 2.5 5 10 15 20 25
Kilometers

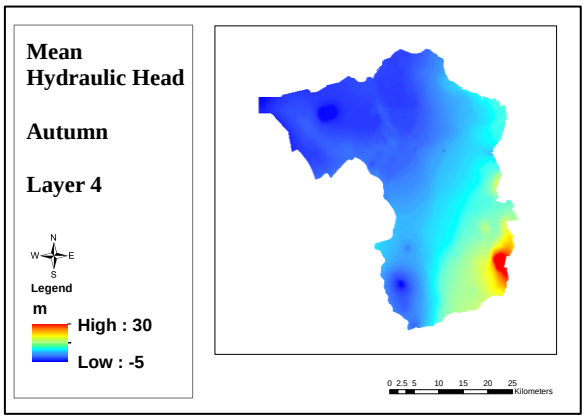
Mean
Hydraulic Head
Autumn
Layer 4
Legend
m
High : 30
Low : -5
0 2.5 5 10 15 20 25
Kilometers

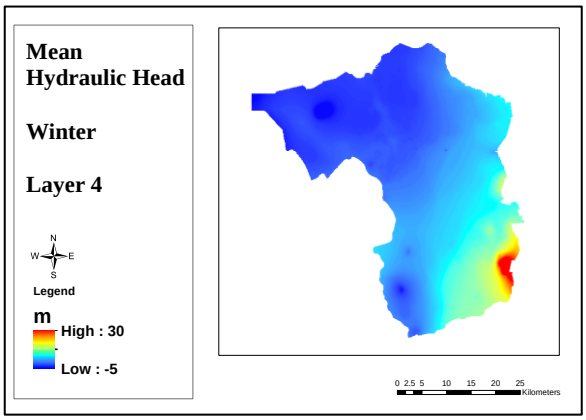
Mean
Hydraulic Head
Winter
Layer 4
Legend
m
High : 30
Low : -5
0 2.5 5 10 15 20 25
Kilometers

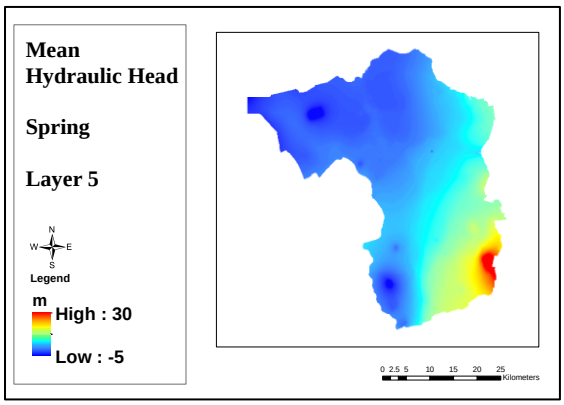
Mean
Hydraulic Head
Spring
Layer 5
Legend
m
High : 30
Low : -5
0 2.5 5 10 15 20 25
Kilometers

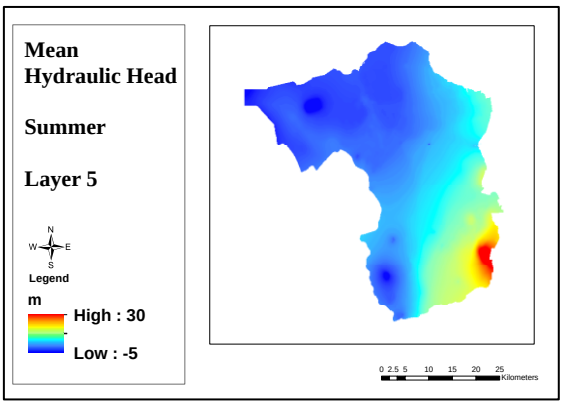
Mean
Hydraulic Head
Summer
Layer 5
Legend
m
High : 30
Low : -5
0 2.5 5 10 15 20 25
Kilometers

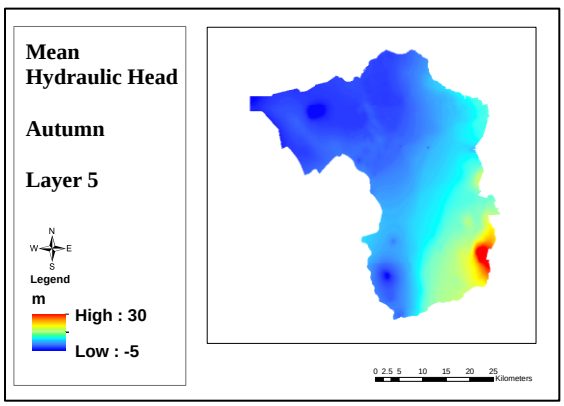
Mean
Hydraulic Head
Autumn
Layer 5
Legend
m
High : 30
Low : -5
0 2.5 5 10 15 20 25
Kilometers

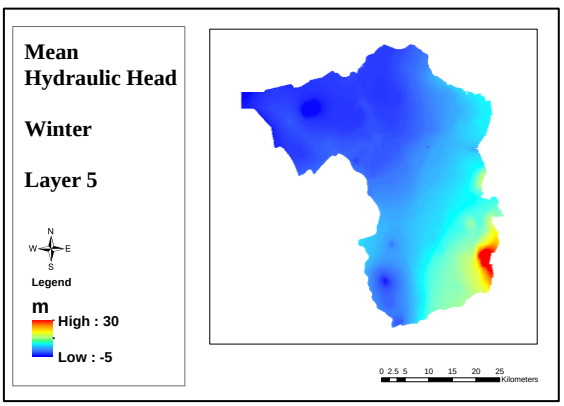
Mean
Hydraulic Head
Winter
Layer 5
Legend
m
High : 30
Low : -5
0 2.5 5 10 15 20 25
Kilometers

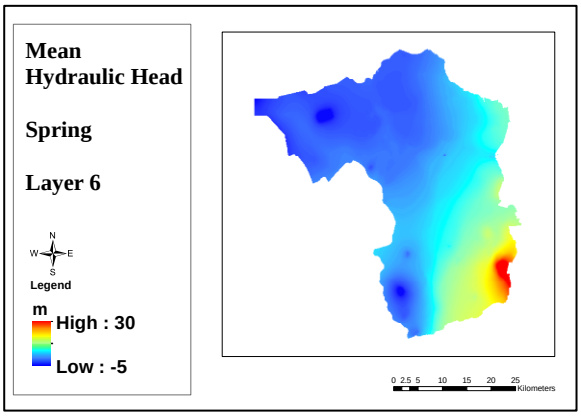
Mean
Hydraulic Head
Spring
Layer 6
N
W
E
S
Legend
m
High : 30
Low : -5
0 2.5 5 10 15 20 25
Kilometers

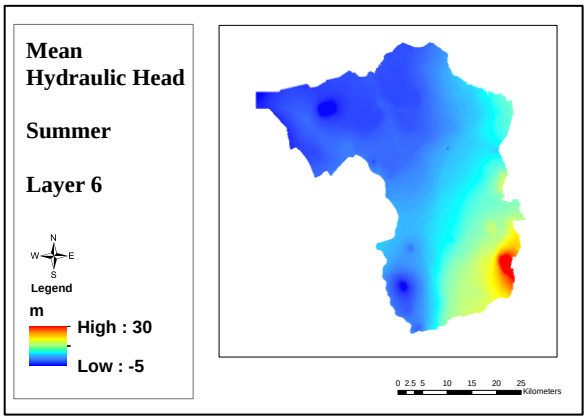
Mean
Hydraulic Head
Summer
Layer 6
N
W
E
S
Legend
m
High : 30
Low : -5
0 2.5 5 10 15 20 25
Kilometers

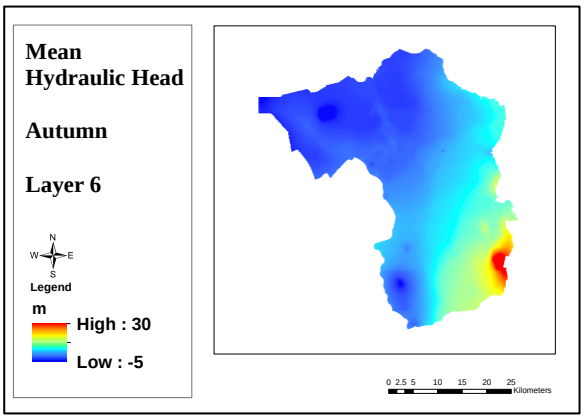
Mean
Hydraulic Head
Autumn
Layer 6
N
W
E
S
Legend
m
High : 30
Low : -5
0 2.5 5 10 15 20 25
Kilometers

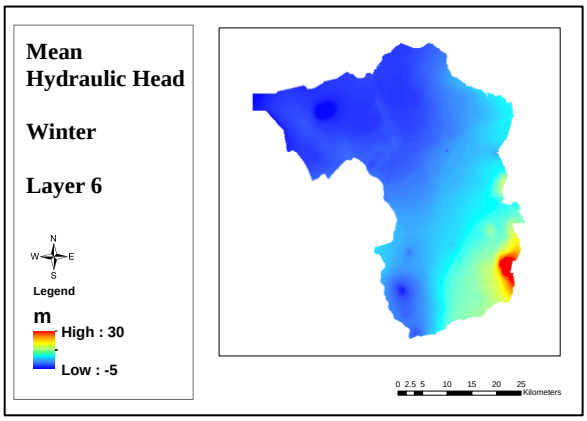
Mean
Hydraulic Head
Winter
Layer 6
N
W
E
S
Legend
m
High : 30
Low : -5
0 2.5 5 10 15 20 25
Kilometers

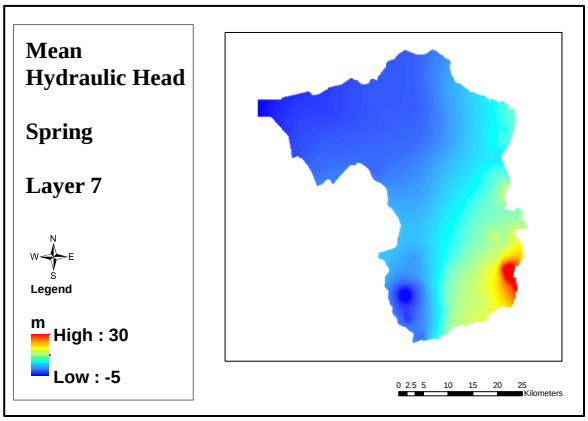
Mean
Hydraulic Head
Spring
Layer 7
N
W
E
S
Legend
m
High : 30
Low : -5
0 2.5 5 10 15 20 25
Kilometers

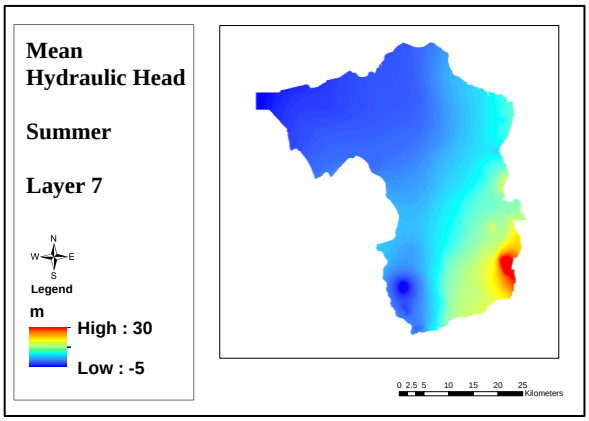
Mean
Hydraulic Head
Summer
Layer 7
N
W
E
S
Legend
m
High : 30
Low : -5
0 2.5 5 10 15 20 25
Kilometers

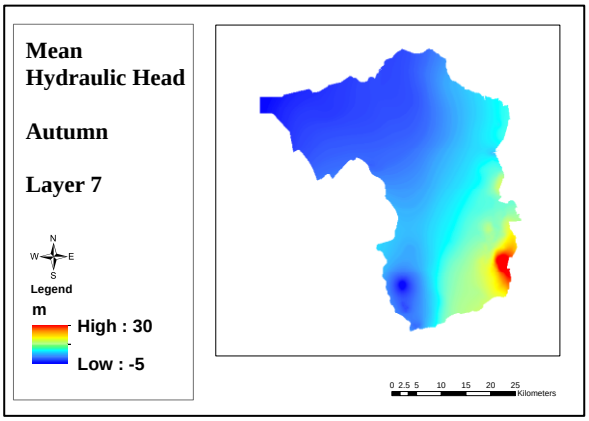
Mean
Hydraulic Head
Autumn
Layer 7
N
W
E
S
Legend
m
High : 30
Low : -5
0 2.5 5 10 15 20 25
Kilometers

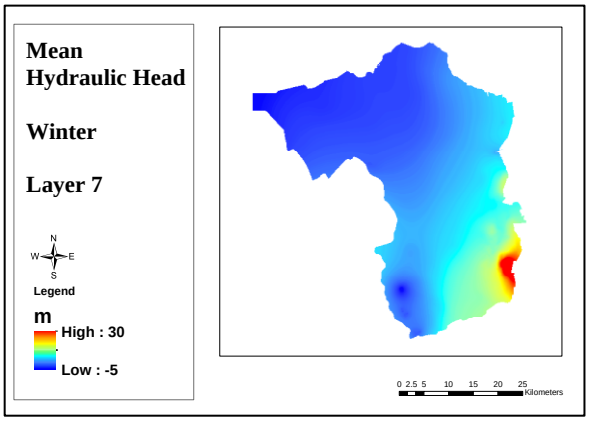
Mean
Hydraulic Head
Winter
Layer 7
N
W
E
S
Legend
m
High : 30
Low : -5
0 2.5 5 10 15 20 25
Kilometers

APPENDICES 4, The meeting in the Waterschap Groot Salland